Winter 12-3-2020

The Magic School Bus

Thomas Murdoch
Kennesaw State University

Hassan Hassan
Kennesaw State University

Nardeen Saleb
Kennesaw State University

The Magic School Bus (FDR)

Team: The Magic School Bus

Due: DEC/3rd/2020

Member:

Thomas Murdoch: Product Manager

Hassan Hassan: Engineering Manager

Nardeen Saleb: Software Leader

I) Abstract:

This report recreates the Fairey Rotodyne in modern, electric form. Extensive research into the market requirements and history of the autogiro are presented as justification for the implementation of such a design. The design criteria and mission profile are selected in order to compete with inter-city commuting in the range of 20 to 30 statute miles or with longer range travel at roughly 100 miles. Cost estimations are also made in order to gauge the feasibility of this design from an economic standpoint. Achieving the design criteria and desired mission profile are done through numerical integration and analysis through CFD to optimize the initial design detailed below. The results that we found show that this is a feasible design worthy of further investigation.

II) Executive Summary:

This summary is on the conceptualization and initial design process of a theoretical aircraft based off the Fairey Rotodyne aircraft first made in the late 1950s. The modernized version would be reduced in passenger capability and range and utilize an electric propulsion system making it an appealing alternative to the environmentally conscious. It is envisioned as an alternative to daily inter-city commuting or from suburbs to metropolitan cities. This summary gives greater detail on the historical background of the autogiro, the perceived need in the marketplace, important literature used, design process, success criteria, power system implementation, economic calculations, controls, weight, aero calcs, and range calculation and future recommendations.

Market demand:

Drivers across the United States spent a great deal of time commuting to work before the pandemic. For example, in Atlanta, the average driver would spend nearly $180,000 and drive 288,000 miles in a 45-year career. This is an unacceptable amount of time spent not even working for your income, but just getting to your job. It is expensive to the commuter in terms of both time and money. This paper seeks to propose an aircraft that would be suitable to replace commuting in terms of affordability and time savings for most people. There are many current efforts in similar spheres such as the flying taxi which is applicable to travel within the city. Many manufacturing/engineering giants are involved with this such as Hyundai and Uber. Uber also offers helicopter rides on demand. However, both approaches only fit a low amount of people thus increasing the cost burden on each person. Our proposal is to have a flying bus of sorts that would be able to hold a greater amount of people that would defray the costs away from the individual consumer. There is also interest in the autogiro in the realm of flying taxis due to the extremely safe nature of the autorotating rotor. The team also thinks that it could be extended for inter-city travel.

Aircraft Type:

Initially, a qualitative review of the various types of aircraft was carried out via a decision matrix comparing a traditional helicopter, fixed wing, and hybrid aircraft. It was determined from this that the hybrid aircraft should be pursued. The decision to purse an electric system was also determined in the same manner. The autogiro hybrid was chosen due to its high level of safety as well as the inherent fixed wing benefits of the hybrid design. A hybrid aircraft was then searched for that is similar to our envisioned approach and requirements. Two such examples were found. These were the Fairey Rotodyne and the Jaunt Air Mobility Journey Air Taxi. The former was more influential because it is closer to our desired application of inter-city travel with a higher passenger capability than the latter.

Design Process/Rationale:

Based off the market research done and the type of aircraft is selected, numerical calculations are performed to determine the aerodynamic characteristics of the aircraft. Design language from similar aircraft is considered. A configuration is come up with and the power requirements/operational range is determined. After power and range are determined a redesign is done to optimize the range, either by weight reduction or by modifying a lifting surface such as increasing the radius of the main rotor. This modification is considered in the context of the entire aircraft and the overall power requirements are then recalculated. For difficult to analyze components such as the fuselage, CFD is utilized via SolidWorks flow simulation. Once the final configuration is determined, another round of CFD is done to tweak the design until satisfaction. If time permits, a scaled down model may be made to test the overall design outside of a virtual wind tunnel.

Success Criteria:

Based on the market needs detailed above, the following success criteria were determined. First is a passenger capacity of 20 with 2 pilots on board. The maximum operational range would be 100 miles with 25 miles of reserve range capacity. VTOL capability is a must to operate in crowded environments such as cities. Cruise altitude should be at 5000 ft and at cruise speed should be 115 kts. A fully controlled landing in a full power loss scenario should be easily achievable through autorotation of the main rotor and all of this should generate no greenhouse gas emissions.

Power System Implementation:

The motors selection was based on the performance needed to achieve the minimum success criteria. The method used to select the best motor is technique for order preference by similarity to ideal solution, also known as (TOPSIS). The TOPSIS method can be applied for variety of project for selecting the best optimal choice from the inputted options. TOPSIS tool works by creating a hypothetical to ideal solution for a specific problem in our case it is selecting the appropriate motor for an Autogiro. The tool compares the given motors with a positive and a negative hypothetical ideal solution. The positive and negative hypothetical solutions are based on the customer preference in the form of selecting a weight to each criterion. The best alternative option has the shortest to the positive ideal solution and farthest away from negative ideal solution. The final step is rank the best option, which is the closest to one, all the way to the least suited option which is the closest to zero or the farthest from one. Some advantages to using TOPSIS tool that its very simplicity and has indisputable ranking method because it's based on the input values and weights. Some disadvantages of using TOPSIS it heavily depends on the weight's preferences, solution highly depends on the input values for each alternative, criteria have a monotonically decreasing or increasing utility to decision maker.

Weight Balance

SoildWorks software was used to arrange the layout of the autogiro. The structure of the autogiro in many cases could be approximated as symmetrical and able to be ignored throughout this process. The mass of the seats, propellers, motors, and batteries were the main factors in ensuring that the center of gravity lined up with the center of lift.

Economics:

The economics of the aircraft were done using very rough estimations of land price, facility, equipment, maintenance, and staff. The equivalent annual costs from an initial investment of 2 facilities and 3 aircraft each having a total of three battery packs, were compared to the tickets sold per year. Flights were assumed to happen 18 times (1 way) per day per aircraft. Each flight would have every seat filled and would operate 365 days per year. Marginal acceptable return rate was set to 20% to account for the risk aspect of this enterprise. Ticket prices were found to be $55.2, $40.97, and $37.32 for a breakeven point of 5, 10, and 15 years. It is important to note that the ticket is one-way. Also, if flights per battery pack were reduced from 3 to 2, the second facility could be reduced greatly in terms of cost, but this was not a scenario calculated for.

Weight/Aero Calculations:

Weight calculations are difficult to do initially. This difficulty is in the fact that there is no real modern analogue to compare this to. Therefore, instead of estimating weight based off similar aircraft, the weight was estimated by comparing various components of the aircraft to similar parts found on other aircrafts and using these weight estimations as design limits for each part. Using this design, we estimated a total mass of 8586.687 kg (84.2354 KN). The various components in this estimation include the weight of the electric motors and their drivers (434.73 kg), passengers with their seats and luggage (2189.19 kg), rotor (454.5455 kg), propellers (109.0909 kg), and fuselage (2272.73 kg). These values were rough, conservative estimations where the actual weight in real life would likely be less. The battery weight was determined to be a total of 534.6155 KWH with a KWH/kg value of 0.171. Total weight of the batteries came out to be 3126.406 kg. It is important to note that the KWH/kg value also accounts for the weight of the battery casing and a drivetrain efficiency of 90% due to the high efficiency electric, direct-drive system.

Rotor calculations were done iteratively through a spreadsheet. The rotor was numerically calculated in excel using basic blade element momentum theory (BEMT) and included an accounting for tip loss via Prandtl's tip loss function. While similar in many ways to the helicopter, the autogiro rotor blade has a few distinct differences. For instance, the blade of the autogiro is better optimized with a positive twist instead of a negative one. Also, the relative size of the autogiro rotor is larger to give a lower disk loading value which helps to reduce descent rates and make it easier to achieve autorotation. With these key differences in mind, the final design of the main rotor blade is as follows; Radius of 11.75 meters, an RPM of 140, an initial angle of 0 degrees with a linear +9 degree twist, two total blades and a linear taper ratio of 3:1 with an initial chord of 1.67 meters. Power requirements are 948.94 KW in hover and 1032.86 KW in a 1 m/s axial climb. This gives a disk loading of 194.25 Pa in hover and is halved during cruise due to the lift generated by the fixed wing. In the event of a full power loss, the vertical descent rate is found to be 16.53 m/s but this can be reduced with some forward movement. For example, a forward velocity of 15 m/s would correspond to a vertical descent rate of 6.94 m/s. In cruise the H-force from this rotor roughly corresponds to 3 KN of drag.

Propeller Calculations were done in nearly an identical fashion as the rotor calculations. The only difference being that the propeller blade was simulated as an ideally twisted rotor with the inner 20% being cut off due to the propeller hub. The propellers were calculated to be a 3 bladed system, with a radius of 1.5 meters, a chord length of 0.15 meters, and operates at 1900 RPM. Airfoil properties were based off generic thin airfoil theory results. The propellers were placed on the tips of the wings as well as the nose of the aircraft. Wing tips were selected because that would allow for the greatest moment arm to counteract the torque from the main rotor during VTOL. Designing around the use of variable pitch propellers allowed for a constantly changing angle of attack to optimize power requirements.

Range Determination:

The calculations for range determination were relatively simple. First, the KW required for each flight regime was calculated. From here the total time for per maneuver was calculated via forward velocity and distance covered. This yielded a KWH per flight regime. The regimes are as follows, VTOL (41.46 KWH), forward climb (43.99 KWH), cruise, and forward descent (18.46 KWH). Cruise was found to be the difference between the allotted KWH in the weight estimation (534.6155 KWH) and the total KWH from the VTOL, climb, and descent phases. This came out to be 534.6155 KWH which matches the weight allotment and is used to find cruise distance. Breaking down each flight regime in terms of distance, there is a total range of 127.44 statute miles. 9.69 of which are from climb and 1.89 of which are in descent. The difference is 115.85 miles which is cruise distance. Cruise distance is shortened by an emergency range allotment. Total time in the air is roughly 1 hour. It is important to note that this range calculated is for a long-distance route where the destination is roughly 100 miles from the start. Overall time in the air would of course be reduced due to there being more landing/take offs.

Future Recommendations:

There are a great many things that are left to do with the overall design of this aircraft. The preliminary design is completed and should be used as a basis for further development. Specifically, regarding the rotor, the hub design needs to be designed, better airfoils selected, composite structure design, and more. For the propellers, actual designs need to be analyzed instead of approximations although this does allow for preliminary sizing and power determinations.

Conclusion:

There is a great deal of promise in this concept. This aircraft managed to achieve its goals even when not fully optimized with conservative weight estimations. The aircraft is capable of inter-city commuting with a passenger capacity of 20. It can get its passengers to its destination at an average speed of about 125 miles per hour in safety, high above traffic. The team believes if serious development were undertaken on this design it would be a viable means of transportation.

Table of Contents

IV) Table of Figures:

V) Table of Tables:

[This Page Intentionally Left Blank]

1.0) Chapter 1: Overview and Background

1.1) Introduction:

The earliest reference related to vertical flight dates to 400 BC in the Chinese civilization, where children used bamboo to make helicopter concept/style toy to play. The toy consisted of stick the size of wood pencil as a base and used to spin a wood attachment and as the attachment spins it generates lift also known as Bamboo copter [1], [6].

Figure 1 Chinese Bamboo Helicopter [2]

Figure 2 Playing with Bamboo Helicopter [2]

In the early 1480's, Leonardo da Vinci created his iconic design known as "Aerial screw" and this is considered to be the next big step toward vertical take-off and landing as it capered the attention of many famous researchers, engineers, for the next few hundred years [3], [6].

Figure 3Leonardo DaVinci's "Aerial Screw" [3]

In the year 1861, Gustave de Ponton d'Amecourt the French inventor demonstrated a small steam powered model. The model failed to successfully vertically lift off; however, Gustave incorporated aluminum in his model which is strong light weight material that is widely used in the aerospace industry and also, he coined the term "helicopter" in the patten when describing his model [4]. Then, in the year 1878 an Italian man know by Enrico Forlanni build a steam powered, unmanned, with VTOL capabilities. The model was successful to vertically take off and rise to the height of about 40 ft (12 meters) and hover for about 20 seconds then land [5], [6].

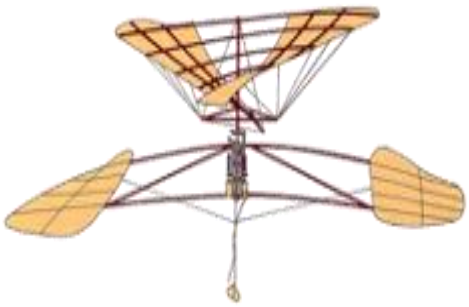

Figure 5 Gustave's Design in flight [5]

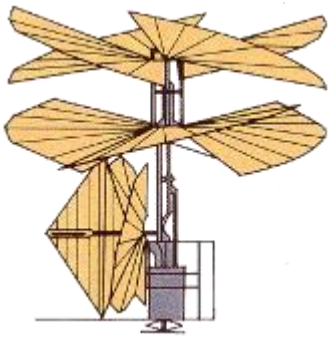

Figure 4 Gustave's Steam Powered Design [4]

By the 1920s a Spaniard by the name Juan de la Cierva had invented the first Autogiro. Autogiro or Gyrocopter consisted of vertical mounted rotating propeller that is freely spinning to generate lift and sets of engines mounted of the wings for forward motion (thrust). Juan idea was to invent an aircraft for vertical takeoff and landing combined with forward motion. [7].

Figure 7 Juan de la Cierva [7]

Figure 6 First Autogiro [7]

This project was inspired by the Fairey Rotodyne. This unique aircraft is an autogiro, while still having wings and propellers. The purpose of the main rotor is to reduce the amount of lift the wings need to produce. This innovative vehicle failed due to excessive noise and economic issues. The Fairey Rotodyne was ahead of its time, as tip jets weren't quiet.

Figure 8 Fairey Rotodyne (Autogiro) [18]

Another aircraft that was considered in this project was the Kamov Ka-22 “Vintokryl.” This was a very large autogiro that was to be used for military purposes, however this was also unsuccessful as it crashed twice and lost public trust.

Figure 9 Kamov KA-22 “Vintokryl” (Autogiro) [12]

The V-22 Osprey was researched when a tilt rotor was considered. This kind of aircraft can take off vertically and once in the air, the rotors tilts forward to generate thrust. The benefit is that this aircraft is much faster than a typical helicopter while still having VTOL capabilities [17].

Figure 10 V-22 Osprey (Tilt Rotor) [17]

The specs from a smaller autogiro, the Gyro-1, was also researched. The benefits of this aircraft are that it is very lightweight and is less prone to bunt-over; a phenomenon that occurs when the rotor is unloaded in air with the propeller still operating. If the line of force of the propeller is above the center of gravity as it more commonly is in pusher propeller type gyros, the aircraft might flip in the air and crash with no chance of recovery.

Figure 11 Gyro -1 (Autogiro) [19]

1.2) Overview:

The Autogiro design was fully integrated with electrical motors and sets of battery system. Our autogiro consists of three high power motors (Magni 500 each rated for about 751 hp). Each one powering its own propeller. There is a propeller on each wing tip and one on the nose of the aircraft. Also, there is another set of smaller motors (YASA 750R each rated for 135 hp), the motors are stacked together and power the main rotor for vertical thrust. This design idea is promising as it combines the best of both worlds by having the power source be green with no emissions while having the safety of an autogiro and the speed of a fixed wing aircraft, with far less maintenance required as compared to traditional combustion aircraft. The batteries used in this design are state of the art lithium-ion batteries produced by Tesla motors co. The mission profiles for this aircraft is shown in [Fig.1].

Table 1 Power and Propulsion Parts of the Design

QNT.	Part Name
3	Magni 500 (Big E-Motor)
6	YASA 750R (Small E-Motor)
1	Rotor for VTOL
3	Smaller propellers for forward thrust
N/A	Panasonic 2170 Battery

1.3) Objective:

This aircraft was envisioned as an alternate method of transportation. This proposed design is developed at the lowest cost, be environmentally friendly, have robust safety measures built in, and feature a simple structure. This method of transportation may be used in addition to existing public transportation, to encourage more people in congested cities to choose public transportation over using their own vehicles.

1.4) Justification:

According to the Atlanta Journal-Constitution “the average American commuter who drives works spend roughly 11,250 days working/commuting over the course of a 45-year career, spends $108,727 on gas and maintenance costs, and drives about 173,203 miles related to work [20].”

Atlanta drivers spends an average of $182,886 and drives about 288,000 miles during the same 45-year career time period. “more than any other city in the survey, Dallas and Huston tied for the second place with $174,314 and 274,500 miles driven [20].”

Moreover, according to the INRIX Atlanta has landed the highest rank on the worst commutes in the states and the eighth-worst traffic congestions in the world in 2016 and 2017 [20].

Bigger cities such and New York city, Los Angles, and Chicago are bigger in area and have much bigger population, however, their public transportation is much more efficient with lots of routes and most locations can access with the public transpiration. Unlike such big cities which have developed their own unique systems of mass transportation, Atlanta is still growing cities and such efficient transportation systems and Infrastructure can’t keep up with the demands of the population and the

growing city. Thus, we are proposing our idea of Autogiro bus to have smarter, cost efficient, and effective city to city transportation.

If a company were to reach out to a company or governmental entity such as MARTA, this aircraft may be added to that entity's current system to encourage the use of public transportation and reduce traffic congestion in cities like Atlanta, while also reducing pollution created by excessive cars usage.

1.5) Project Background:

Modern efforts are directed at the flying taxi. For instance, the Hyundai manufactured flying taxi concept for Uber that would fit five including the pilot [8]. This low number contributes to the cost of each seat to the consumer. An example of current cost to the consumer is the $200 to $225 per seat for an Uber Helicopter ride which is on demand. The Autogyro is copiable of taking passengers from Lower Manhattan to JFK and includes car service to and from the helipad at each end [9].

The price with production volume is of course going to go down but there is a limit to how cheap a seat can be if there can only be four paying passengers per flight. The team thinks that there is a greater possibility to quickly reducing the cost per seat with larger aircraft capable of carrying up to 5 times the number of paying customers. It would also be targeted at the suburbs with a goal of decreasing rush hour traffic like MARTA. Ideally it would fill the role of the inter-city/commuter bus.

There is also a great deal of interest in the idea of the autogiro with many espousing the unique qualities of this type of aircraft. There are many possible applications it could be used for such as intra- and inter-city travel, border patrol automation, and transportation to remote areas [10]. An example of a modern autogiro taxi is the Journey autogiro developed by Jaunt Air Mobility [11]. The Journey autogiro takes advantage of a proprietary technology that is used to slow the main rotor speed called ROSA. While this design is of great interest it is different from our goals mainly due to the capacity of this aircraft. It is only able to carry four passengers like the Uber-Hyundai aircraft while our goal is to have a capacity of twenty

1.6) Problem Statement:

Design an electrical passenger transport hybrid gyroplane. The gyroplane must be designed for city to city flights and commuting for twenty passengers.

2.0) Chapter 2: Literature Research

2.1) Literature Reviews:

The Autogiro (Autogiro) is a rotary wing aircraft which utilized propeller for horizontal thrust. This unique aircraft design was created after the first world war “as a safe alternative to the airplanes”. The Autogiro works by using the rotary style propeller for the vertical take-off and landing (VTAL) when the desired altitude reached, power to the rotary propeller then switched to power the smaller propellers for thrust. The design style resembles the characteristics of both helicopter and airplane and the characteristics of the helicopter and airplanes are very distinguished from one another. The autogiro has the characteristics of a helicopter during the take-off and landing phases and during the cruise phase it utilize similar characteristics of an airplane, however the rotor is generating some lift due to the free stream of air [21].

Autogiro pitch and control: Autogiro is like a helicopter in appearance; however, its main rotor operates by a different aerodynamic principle, moreover the plane take-off backward with the help of main rotor pitching mechanism to generate enough lift needed at takeoff. Thus, with respect to the flight direction under normal flight conditions the Autogiro takes-off rearward which when compared to a traditional helicopter which typically takes-off toward its flight direction (destination). During a steady flight (cruise) there isn’t any power being supplied to power the main rotor which means there aren’t any forces (mainly torque) transmitted from the propeller to the frame of the aircraft. Moreover, since Autogiros doesn't transmit any torque to the airframe which makes torque-balancing tail useless which is one of the main differences between gyrocopter and helicopters. Autogiro pitch is usually controlled by adjusting the main rotor tips-path. During a straight level flight at low speeds, the main propeller rotor is tilted backward to maintain air flow the rotor and prevent air separation and turbulent airflow; moreover, as the rotor is tilted backward the rotor tips-path's angle increases this contributes to the increase in the rotor’s induced drag. Thus, the throttle/ power must increase to maintain straight, level, and slow speed flight. In a low speed steady flight, the rotor is shifted all the way backward to maintain and provides the lift needed for the steady level flight. However, in order to recover from the low speed flight, the autogiro need to descend creating upward flow through the main rotor (autorotation) increasing the blades rotational rate. In the case that a enough altitude has not been reached before but the pilot created some upward flow through the main rotor, descent or recovery may be attained but the autogiro most likely will impact with the ground [22].

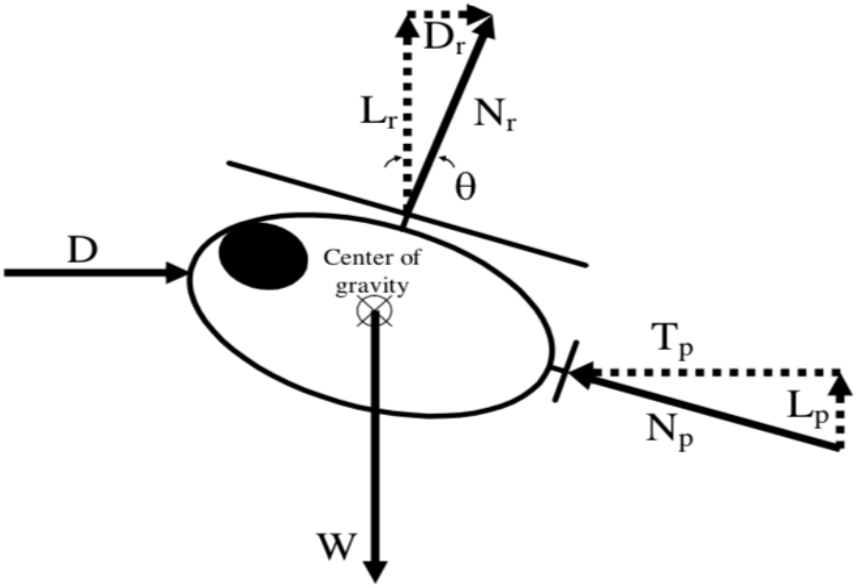

Figure 12 Forces on Helicopters [22]

$$\sum F_x = D + D_r - T_p = 0$$
$$\sum F_Y = L_r + L_P - W = 0$$
$$M_{CG} = 0$$

Where D is the drag force, D_r is the induced drag by the rotor tilt-back, T_p is the thrust produced by the propeller rotating, L_r is the vertical lift generated by the propeller rotating, L_P is the component of propeller thrust acting in the vertical (Y-axis) direction. W is all the weight of the autogiro before take-off, and finally M_{CG} is the sum of moments about the plane's center of gravity.

Flight Path Control System of Unmanned Autogiro: this research paper used flight tracking control system for unmanned autogiro and designs the controlled based on the control characteristics of the unmanned autogiro. The flight path control system is designed to reduce the loss of lift forces during turning and at level steady flight. This autogiro is in the light aircrafts category which means its lightweight single prop-engine for thrust and still uses main rotor for VTAL capabilities. Since this unmanned autogiro is a single prop-engine which is mounted at the noise of the aircraft during acceleration, turning, and during roll the amount of propeller twist causes significant and present torque on the aircraft frame. To reduce the influence of propeller anti-twisting effect, a feedforward control method of the propeller rolling rudder (during throttle changing). To reduce the amount of slide slipping and achieve coordinated turns, a hybrid control strategy for the yaw rudder and rolling rudder of propeller is developed. The control system has proven to effectively control the altitude and horizontal path of the unmanned autogiro, with control accuracy of better than ±5 meter [23].

Gyrocopter rotor blades have a smaller cord length and longer span compared to helicopters blades. National Advisory Committee for Aeronautics (NACA) 8-H-12 gyrocopter rotor blade profile, unsymmetrical airfoil sections were used for this research. An attempt has

been made in this work to investigate the effect of ribs and spar elements in response to the applied load. Three possible modeling alternatives were studied to predict the actual induced stress and deformation of the blade: Model I is by considering the blade shell part only, Model II is blade shell with 25 numbers of ribs and without the spar element, and Model III is blade shell with 25 members of ribs and with spar element. The rotor blade was sized based on a single-seat open frame and high-wind-start gyrocopter. Structural static analysis has been carried out to evaluate the strength of the composite rotor blade using ANSYS Workbench 15. The results show that among these three proposed models, Model III had registered minimum Von-Mises stress and deformation. Also, the result reveals that considering ribs and spar elements during the analysis of the gyrocopter blade is crucial because it helps identify the actual induced stress and deformation. The predicted value of induced stress and deformation is closer to the fundamental values, that helps the designer not to overdesign the parts. Consequently, the main drawbacks related to overdesign increase in weight and the cost is minimized; thereby, the operational production is improved and as efficient as possible [32].

The work and the study in this article describe integrating a manned autogiro model in a simulation framework for unmanned vehicles. This framework provides several advantages for the development process through a sensible set of requirements and principles, namely: continuous integration, flexible testing and validation, and simple means of operation. As a result, our framework enables the constant development of new flight maneuver/flight automation algorithms for our optionally piloted autogiro testbed, such that the feedback time from lessons learned during simulation trials or flight tests is short [33].

Despite current research advances in aircraft dynamics and increased interest in the slowed rotor concept for high-speed compound helicopters, autogiro rotors' stability remains partially understood, particularly at lightly loaded conditions and high advance ratios. In autorotation, a rotor blade's periodic behavior is a complex nonlinear phenomenon, further complicated by the fact that the rotor speed is not held constant. The analysis done in this article aims to investigate the underlying mechanisms that can lead to rotation-flap blade instability at high advance ratios for a teetering autorotating rotor. The stability analysis was conducted via wind tunnel tests of a scaled autogiro model combined with the numerical continuation and bifurcation analysis. The investigation assessed the effect of varying the flow speed, blade pitch angle, and rotor shaft tilt relative to the flow on the rotor performance and blade stability. The results revealed that rotor instability in autorotation is associated with the existence of fold bifurcations, which bound the control-input and design parameter space within which the rotor can autorotate. This instability occurs at a lightly loaded condition and at advance ratios close to 1 for the scaled model. Finally, it was also revealed that the rotor's inability to autorotate was driven by blade stall [34].

An autogiro rotor blade for generating lift by autorotation defines a root-side inner profile region with a first profile. The internal profile region has a tip-side main profile region with a second profile different from the first profile. A profile depth curve that decreases monotonically in the longitudinal direction of the autogiro rotor blade from the blade root region in the direction of the blade tip. The autogiro rotor blade has a twist having a twist curve that decreases monotonically from the area of the blade root in the direction of the blade tip. The twisted curve has a variable slope in the inner profile region and/or main profile region, and therefore the twist curve is concavely curved in this region [35].

This paper presents a new attitude tracking control scheme for the autogiro. An example unmanned autogiro is built and modeled based on the explicit blade element method (EBEM). To tackle the strong coupling and fast time-varying periodic disturbances, a new attitude control scheme is proposed. The project employs nonlinear dynamic inversion augmented with a derivative-free adaptive neural network to achieve decoupling and fast compensation. To coordinate the aerodynamic control surfaces and non-affine rotor cyclic pitch controls, a rotor-surface control allocator is designed based on the dynamic control allocation method. Numerical simulations illustrate the superior performance of the proposed scheme comparing to conventional PID and derivative-based adaptive controllers in the presence of fast time-varying disturbances [36].

Owing to its ability to alleviate the compressibility effect on the advancing side, the slowed rotor operating at high advance ratios is a critical feature in high-speed compound rotorcraft. A series of wind tunnel tests were conducted in the Glenn L. Martin Wind Tunnel with a four-bladed Mach-scaled articulated rotor. The objective of the tests was to gain a basic understanding of unique features of high-advance-ratio aerodynamic phenomena, such as thrust reversal and dynamic stall in the reverse flow region. In this study, high-advance-ratio tests were carried out with highly similar, non-instrumented blades and on-hub control angle measurements to minimize possible error due to blade structural dissimilarity and pitch angle discrepancy. The tests were conducted at 900 and 1200 RPM, with advance ratios of 0.3-0.9, and a shaft tilt study was conducted at ±4. Pitch and flap motion at the blade roots, rotor performance, and vibratory hub loads were investigated during the test. The test data were then compared with those of previous tests and with predictions from the comprehensive analysis. The air load results were investigated using the complete study to gain insights into the influences of advance ratio and shaft tilt angle on rotor performance and hub vibratory loads. Results indicate that the thrust benefit from backward shaft tilt depends on the change in the inflow condition and the induced angle of attack increment. The reverse flow region at high advance ratios is the major contributor to changes in shaft torque and horizontal force [37].

The textbook “Principles of Helicopter Aerodynamics” by J. Gordon Leishman is a well written text describing the various physical phenomena that occur on helicopters and how to analyze, diagnose causes of, and promote/prevent said phenomena. Chapter three of this text was used to gather equations for blade element momentum calculations utilized in excel. These equations are used to calculate the characteristics of the rotor such as power required and thrust in hover/axial climb [31]

This article was published by NASA and the U.S. Army to investigate the usefulness of large, heavy-lift and high-speed rotorcrafts for both civil and military use. Three main rotorcrafts were further studied for this application; the Quad Tiltrotor (Bell Helicopter), reverse velocity rotor concept (Sikorsky), and the tiltrotor (Boeing). One of the goals was to further increase the accessibility of air transportation system while at the same time reducing congestion. Requirements for this VTOL aircraft included flying quietly, economically competitive with a Boeing 737 aircraft, exploit available air and ground space, have structural efficiency, efficiently hover, and to push state-of-the-art rotorcraft technology. The investigation yielded three designs; the Large Civil Tilt rotor (LCTR), Large Civil Tandem Compound (LCTC), and the Large Advancing Blade Concept (LABC). [16]

This journal mentions that “steps are being taken to arrange for tests in taking off and landing autogiros from roofs of large buildings in the heart of London” which is what this project hopes to accomplish as well. The fact that this journal was written in 1931 brings up the point

that autogiros, though old, have a lot of potential that has yet to be implemented in a large scale. [33]

The textbook “Aircraft Design: A Conceptual Approach” is a very useful resource for this project. One of the especially useful chapters was able to assist in design of the internal structures of the aircraft, such as specific design of the location of seats, aisle heights, and spacing. Other useful information in the textbook include basic calculations for lift & drag, sizing, and weight distribution. The book also provides a rough understanding of the steps that should go into designing an aircraft, as it is not simply one step after the other, but rather doing multiple calculations at once that all effect each other [24].

The report “Fuel Cell and Battery Electric Vehicles Compared” is written to compare the different attributes of electric, hybrid, and fuel cell cars. Here we were able to compare the relative energy densities of these systems and gave us cause to look at hydrogen fueled turboprop or turboshaft engines. [34]

Published in the journal of ocean engineering in 2004, the paper “Significance of blade element theory in performance prediction of marine propellers” discusses various types of blade models as well as their pros and cons. Early on it discusses blade element theories including the blade element momentum theory used in this analysis. However, it rather quickly determines that the drawbacks of blade element momentum theory such as inaccuracy at large stall conditions and a general under-prediction of torque and power as well as an over-prediction of thrust can be improved if the blade element theory is broken into a panel/integral boundary layer method (IBLM). “Here the properties of each blade profile are not postulated beforehand but the equations for profile lift and drag coefficients are integrated with those describing the momentum and blade/fluid interaction phenomena.” The resulting procedure should not require a large amount of iterations to converge while considering the effect of the actual values of the incidence angles and Reynolds numbers. The author later uses his proposed method to analyze a known propeller. He again analyzes the same propeller using a three-dimensional viscous calculation to compare the results of the two methods and give pros and cons [35].

3.0) Chapter 3: Design Approach and Methodology

3.1) Problem Solving Approach:

After the type of aircraft was determined, hand/numerical calculations were done to find the required power for a determined weight and rate of climb, and rotor blade sizing. Other parameters such as the drag of the aircraft were determined via CFD in SolidWorks. Each design as it is come up with was calculated and deficiencies were noted. The team then brainstormed to come up with various solutions, these changes were calculated again, and the process would repeat until we were satisfied.

SolidWorks is not very accurate for CFD especially pertaining to airfoils. Ideally, for deeper analysis of the design the aircraft surfaces would be analyzed in a more accurate program such as CATIA.

Finally, we would analyze the aircraft in real life we would 3D print certain parts that we would want to test and use the resources of the aerodynamics lab provided on campus to analyze the design.

3.2) Minimum Success Criteria:

The following list is of our criteria for success. It includes range, payload, flight characteristics, and safety goals.

- An operating range of 100 miles with 25 miles of reserve range capacity.
- 20 passenger capacity with 2 pilots.
- VTOL capable in confined environments such as a city.
- Cruising altitude of 5,000 ft.
- Controlled landing in a full power loss scenario using autorotation of the main rotor.
- No greenhouse gas emissions.
- Cruise speed of 115 kts.

3.3) Project Management:

- Thomas Murdoch: Product Manager
- (Pk) Hassan Hassan - Engineering Manager
- Nardeen Saleb – Software Leader

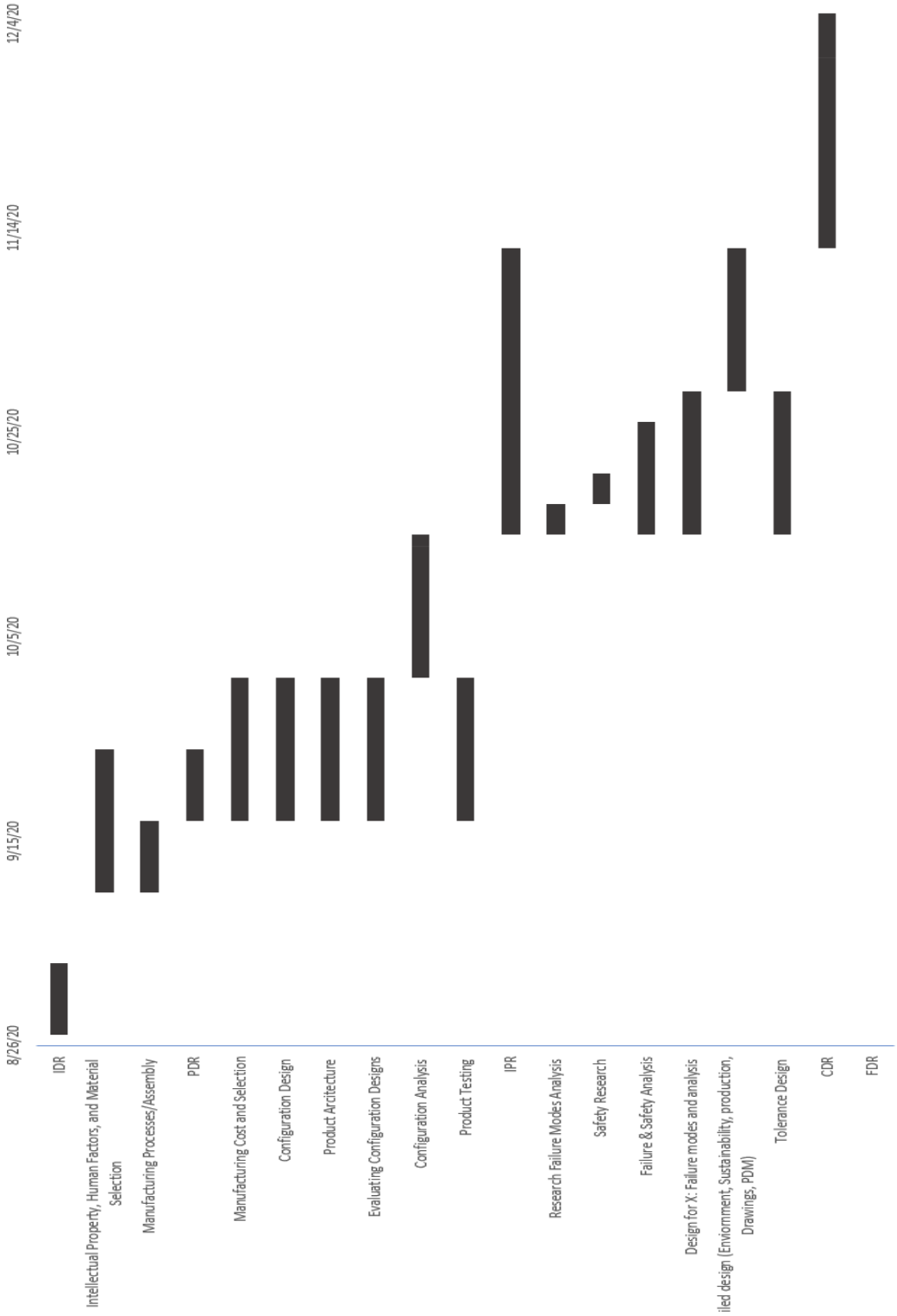

Figure 13 Gantt Chart, Updated Schedule of when tasks were completed

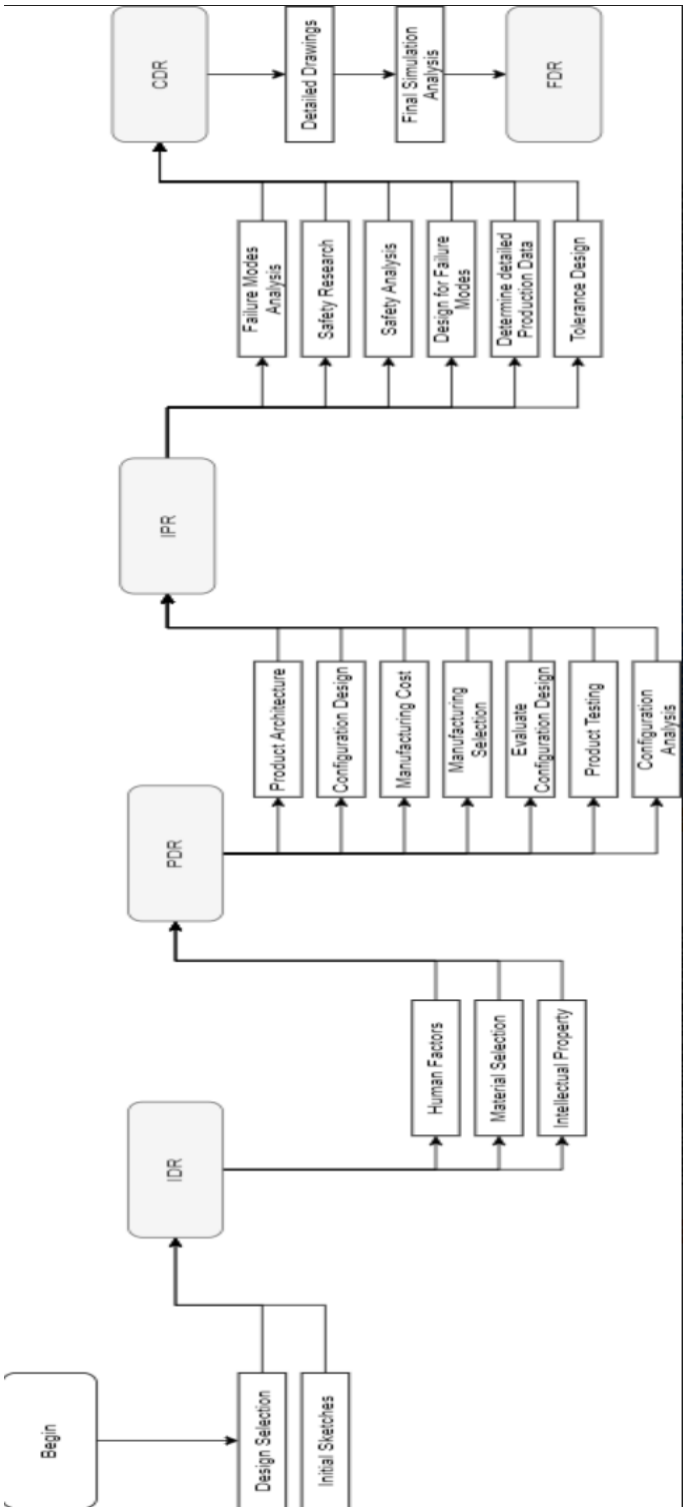

Figure 14 Flowchart, General steps of tasks that were done

3.4) Schedule:

Table 2 Schedule

Task Required	Member Responsible	Completed Day
Research (literature review)	All members	Sep/2nd/2020
CAD Modeling	Nardeen	Sep/16th/2020
Wing Selection	Hassan	Aug/31st/2020
Main Rotor Calculation	Thomas	Aug/17th/2020
Weight Goals	All members	Aug/9th/2020
Control Surfaces	Hassan	Sep/23rd/2020
Flow Chart	Nardeen	Sep/2nd/2020
Mission Profile	Hassan	Aug/26th/2020
Trade Studies	Nardeen	Aug/26th/2020
Weight Re-evaluation	All members	Sep/19th/2020
Main Rotor Re-evaluation	Thomas	Sep/22nd/2020
Wing Re-evaluation	Hassan	Oct/22nd/2020
Revised CAD model	Nardeen	Nov/11th/2020
Forward Propulsion (started)	Thomas	Sep/29th/2020
Tail and Control Surfaces	Hassan	Nov/10th/2020
TOPSIS	Hassan	Nov/11th/2020
Final Main Rotor Designed	Thomas	Nov/11th/2020
Final Propulsion Evaluation	Thomas	Nov/11th/2020
Range Calculations	Thomas	Nov/11th/2020

Table denotes the finish dates (unless otherwise indicated) of important tasks

3.5) Budget:

Table 3 Itemized Bill of Materials for Purchased Parts

QNT.	**Part Name**	**Cost per Item**
3	*Magni 500*	*Pending Response*
6	*YASA 750R and 800V Cascadia Motion PM 150 DZ Driver*	*$25,543.09*
534.62	Panasonic 2170 Battery	*$170/KWH*

The table above lists the prices of components currently available for purchase. Price for batteries is not easy to come by as they are relatively new and used for commercial purposes. However, a website was found quoting a price of $170/KWH, but it is a battery vendor and not the manufacturer [44]. This was used in the price calculations.

3.8) Economic Calculations

The following economic analysis was done with many assumptions. It would be best to take this then with a grain of salt. The analysis was done to determine the price of the tickets to break even in a desired number of years. It is important to note that the information used is not from reputable sources because it was difficult to find such sources.

First the cost of the aircraft was determined by finding a similar helicopter in terms of weight, power, and passenger capacity. The Airbus H175 was found to suit those requirements weighing 7,800 kg, power of 1324 kW, and a passenger capacity of 18 [45]. The H175 uses 2 Pratt & Whitney PT6C-67E [45]. Converting the values from the H175 to our aircraft involved taking the total cost of a new H175 of $17 M [46] and subtracting the cost of the two engines valued at roughly $1 M each based off a related engine [47]. This helps to give an accurate idea of the costs of production, avionics, rotor blade manufacturing, etc. However, it does not give an accurate idea of the costs of certifying and producing a whole new type of aircraft not based off any other model. This was not accounted for, but it is something to keep in mind.

Finding the cost of the electric power system was done as follows. Each motor/driver pair was estimated to cost $25,543.09. This number was a quote from YASA which also applies to Magni motors due to their lack of a prompt reply. Cost of the batteries was found to be $170/KWH with a total KWH of 534.62 per battery pack. Assuming an initial purchase of three aircraft each with two backup battery packs gives a total value of $15.503 M each.

After this, the initial cost of purchasing the landing zones was estimated. The land was estimated based off commercial land costs in Atlanta to be $1.5 M [48]. The cost of the building (hangar) is $3.5 M at $350/SqFt for a total SqFt value of 10,000, enough to hold 2-3 aircraft and have room to repair and work on them [49]. Initial equipment costs were also estimated to be $1 M to include things like fire suppression, baggage handling, aircraft towing, etc. The total cost of each landing zone is estimated to be $6 M. Two of these were assumed to be purchased/developed. Overall, the initial cost is $58,507,632.03.

Recurring costs were then determined such as salary, repairs/maintenance, and miscellaneous equipment costs. In terms of salary, everyone was assumed to have a cost of $25,000 in terms of benefits on top of their salary. Roles determined were 3 mechanics/facility, 1 in logistics, 2 desk-workers/facility, 2 pilots/aircraft, and 1 in IT. Salaries respectively were $70,000, $70,000, $35,000, $100,000, and $50,000. The total annual salary cost was then determined to be $1.73 M. Building maintenance costs were estimated to be $100,000 with miscellaneous costs from equipment and parts to be $50,000. This is a total recurring cost of $1.88 M per year.

Income was then found on an annual basis. Each aircraft can do three legs per battery pack and there are a total of three packs per aircraft meaning a total of 9 legs in the morning and 9 in the evening leading to a total of 18 legs per aircraft per day making a total of 54 per day. The aircraft are estimated to be full on each trip meaning 20 tickets per leg to a total ticket sales of 1080 per day and a total of 394,200 tickets a year if operating 365 days a year. It is important to note that each battery costs roughly $60 to charge fully from the cost of electricity being estimated at $0.11/KWH [50] with each aircraft requiring 6 charges per day. This equated to an electric bill of $1080 per day or $394,200 per year.

MARR (minimum acceptable rate of return) was set to 20% to help attract investors to what is a risky business venture. After all this the cost of the tickets could be calculated.
The first thing to do is to decide upon a desired amount of years until breaking even. The first number of years was chosen to be 5. Then equating the initial up-front cost to an annual value is done as so (58,507,632.03*(A/P, MARR,5)):

$$Equivalent\ Annual = \$58{,}507{,}632.03 * 0.33438 = \$19{,}563{,}782$$

After this the annual cost is added to find a total:

$$Total\ Annual\ Cost = \$19{,}563{,}782 + \$1{,}800{,}000 + \$394{,}200 = \$21{,}757{,}982$$

Dividing the total annual cost by the number of tickets sold per year yields a ticket cost of:

$$Ticket\ Cost = \frac{\$21{,}757{,}982}{394{,}200} = \$55.20$$

It is important to note that this ticket cost is for only 1-way. A commuter would be expected to spend double this at $110.40. Repeating the process for two other intervals of 10 and 15 years. At ten years, the ticket cost is $40.97 each way and at fifteen years it is $37.32 each way.

It is important to remember all the assumptions built into this analysis. The daily operation, consistently full rides, and all the price estimations in production, salary, hangar costs, etc. The prices also do not include the costs of certifying and producing a made from scratch aircraft for public transportation nor does it account for regulatory restrictions. It does not account for the time required to train personnel or construct facilities.

3.9) Power System Specifications

Table 4 YASA 750R Specs

Peak Torque @ 450 A_RMS	790 Nm
Peak Power @ 700 V_DC	200 KW
Peak Power @ 400 V_DC	100 KW
Continuous Torque (40 C coolant)	400 Nm
Continuous Power @ 3000 RPM (40 C coolant)	70 KW (max)
Speed	0-3250 RPM
Peak Efficiency	>95%
Mass	37 kg
Peak Power Density	>5 KW/kg

Through-Shaft Mounting, motors are stackable to increase torque and power. Position and temperature sensors are integrated into the motor. Cylindrical profile with a 368 mm major diameter, 98 mm height, and a 52 mm diameter spline through shaft. Torque and power vs rpm curves are given for both 800 Vdc paired with a 450 Arms controller as well as 400 Vdc with a 400 Arms controller [37].

Table 5 Cascadia Motion PM150 DZ Motor Driver

Operating DC voltage	100-820
Max Continuous Current (Arms)	225
Max Current (Arms)	300
Peak Power Output (KW)	170
Weight (kg)	10

Driver selection was based on recommendation by the motor manufacturer. The driver selected can provide a peak power of 170 KW which means that the peak motor power output is a little below that number. However, without lab testing it is not possible to have accurate numbers for this configuration. Propeller calculations is be done with motor output values only [38].

Table 6 Magni 500 Specs

Continuous Torque (Nm)	2814
Continuous Power (KW)	560
Speed Range (RPM)	1900-2600
DC Link Voltage (nominal)	540

DC Link Voltage Range	450- 750
Motor Efficiency	>93%
Motor Weight (kg)	135

Motor is approximated as a cylinder. This translates to a cylinder with a diameter of 652 mm and a height of 729 mm. These motors do not appear to be stacking and operate individually [36].

Table 7 Magni 500 Drive Specs

Output Power (KW)	170
Efficiency	98.9%
Weight (Est in kg)	<12
Voltage (DC)	400-800

Approximating the driver as a rectangular prism, it measures 369mm x 424 mm x 74 mm [36].

3.10) Alternative Power Sources

One source of power that was researched as an alternative power source was hydrogen. There are two methods as to which hydrogen can power an engine. The first is hydrogen fuel cells, which would be similar to a regular battery, and burning hydrogen, which makes this method similar to combustion. The first method was not appropriate for this purpose, as the battery packs that were used are significantly more efficient than what a hydrogen fuel cell would provide. The costs of a hydrogen fuel cell are also much more expensive than the cost of a regular battery. The second method, though efficient in the sense that it will not release any carbon emission, emits another harmful gas, NOx. This gas has been linked to causing lung diseases in humans, as well as being harmful to the environment. One of the goals of this project is to make an environmentally friendly alternative to the multitude of cars commuting to work each morning, so it would defeat the purpose to cease one harmful gas emission, while releasing another, just as harmful one. [51] [52] [53] [54] [55]

3.11) Resources

Since much of the work that was performed is theoretical, most of the resources are utilized suing software and research articles. The software programs that were most utilized by this team were SolidWorks, Excel, and MATLAB. Other programs could’ve been utilized such as Ansys or ABAQUS but what was used was deemed as enough for our purposes. Information that is accessible in the form of research papers, textbooks, and conference proceedings are available through the KSU library and generally searching online. As for available physical resources, we have the 3-D print shop on campus.

4.0) Chapter 4: Trade Studies

4.1) Mission Profile:

This mission profile describes the different stages that the Autogiro that's expected to encounter during each flight. The first stage is the vertical take-off, which would be the rate of 1 $\frac{m}{s}$. The second stage is the forward climb, which is the transitioning point from vertical take-off after reaching the cruise altitude to horizontal cruise, which involves turning off power to the rotor and supplying power to the propellers to gain thrust. The third stage is the cruise; during this stage, the rotor is spinning freely via autorotation, and power only supplied to the propellers. The cruise stage is at an altitude of approximately 1,500 meters or 5,000 ft, a cruise speed of 115 knots, and a range of 100 miles and 25 miles of reserved range for emergencies. The fourth stage is the forward descent, which involves slowing until the fixed wing stalls while keeping power to the propellers to guarantee a desired forward velocity and thus a desired rate of descent. The fifth and final stage is transitioning from forward descent to vertical landing; this stage involved powering the rotor only to descent to the landing pad at a rate of 1 $\frac{m}{s}$, refer to [Figure 15]. In terms of use as a commuting vehicle of 30 miles in range, the cruising range would be reduced and allow for 3 one-way trips per battery pack.

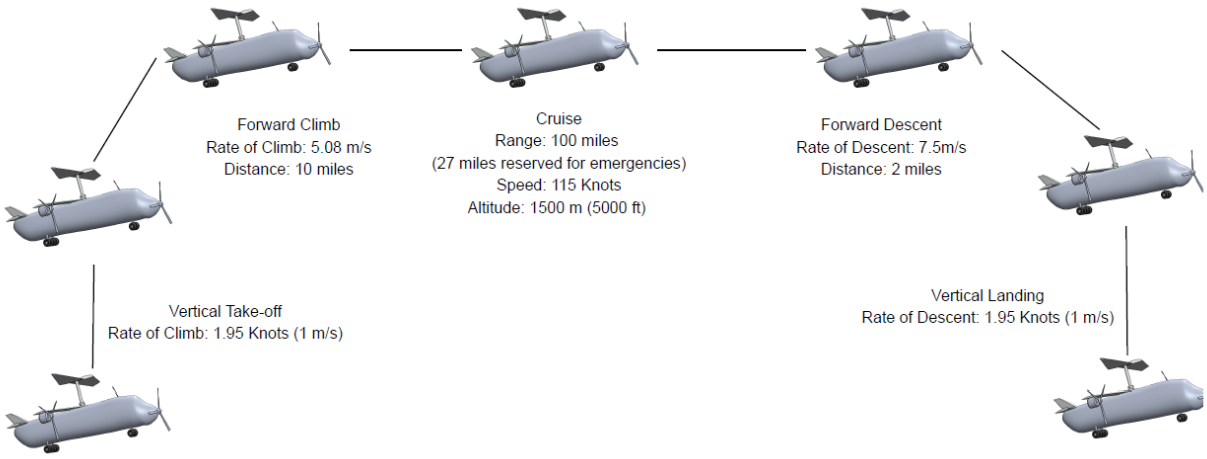

Figure 15 Mission Profile

4.2) Trade Studies

Trade studies were completed on helicopter configuration, power source, rotor configuration and overall design with respect to passenger capacity and power requirements. From these trade studies we were able to conclude that the ideal aircraft would be a compound autogiro in a single rotor configuration that is battery powered. The single rotor was decided upon to reduce design complexity if possible and may have to be revisited. Decisions made on information gathered by market research viewable under the Design Requirements and Research section. It is important to note that the trade studies were qualitative and not quantitative in nature.

Table 8 Trade Study – Rotor Configuration

Criteria	Weight	traditional	Tilt-rotor/wing	Compound
Simplicity	0.2	0.1	0.033333333	0.066666667
Speed	0.25	0.041666667	0.125	0.083333333
Range	0.25	0.083333333	0.041666667	0.125
Maintenance	0.15	0.075	0.020833333	0.05
cost	0.15	0.075	0.025	0.05
Weighted Scores		0.375	0.245833333	0.375
		100	65.55555556	100
With a tie I think that the compound type would be best				
when considering market research as a tie-breaker				

Table 10 Trade Study –Helicopter Configuration

Criteria	Weight	Helicopter	Autogiro	Fixed-wing
safety	0.192308	0.032051282	0.096153846	0.06410256
efficiency	0.153846	0.051282051	0.025641026	0.07692308
EOP	0.115385	0.019230769	0.057692308	0.03846154
Maintenance	0.115385	0.019230769	0.041666667	0.05769231
Low/Slow n touch n go	0.153846	0.051282051	0.076923077	0.02564103
VTOL	0.192308	0.082417582	0.082417582	0.02747253
Cost	0.076923	0.012820513	0.025641026	0.03846154
Total		0.268315018	0.406135531	0.32875458
Out of 100		66.06538895	100	80.9470124
Can see that Autogiro won but fixed wing is second.				
Should investigate the hybrid configuration.				

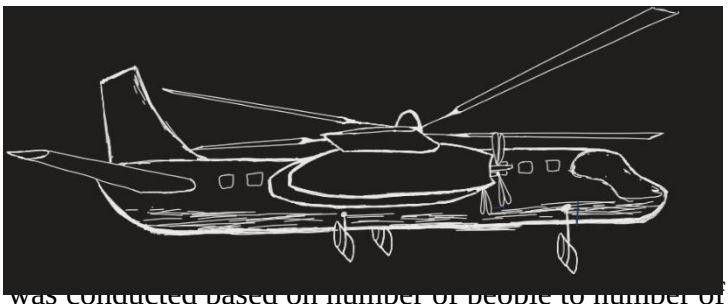

Figure 16 Initial Design Sketch

A trade study was conducted based on number of people to number of needed motors. The above sketch and our power/passenger configurations as shown in table seven. It is very similar in appearance to the Fairey Rotodyne.

Table 10 Overall Trade Study

Description		20P, 3 Motors	30P, 3 Motors	20P, 4 Motors	30P, 4 Motors
Speed	0.1	1	2	3	4
Range	0.05	3	1	2	4
Maintenance	0.025	4	1	3	1
Cost	0.025	1	2	3	4
Safety	0.1	4	4	2	2
Efficiency	0.1	4	4	2	2
Manuverability	0.0125	3	1	2	4
Noise	0.05	4	4	2	2
Low/Slow touch n go	0.0125	4	4	4	4
VTOL	0.1	4	4	4	4
Payload	0.1	2	4	2	4
Reliability	0.1	3	2	1	4
Drag	0.025	4	4	2	2
Lift	0.1	2	3	4	4
Weight	0.05	4	4	2	2
Stability	0.05	2	2	4	4
Total	1	2.9625	3.0875	2.575	3.275

Above table was used to determine the optimal weight/passenger capacity of the initial design. This was later changed to the “20 passenger with 4 motors” configuration due to higher power requirements calculated with blade element theory. Again, this is a qualitative trade study.

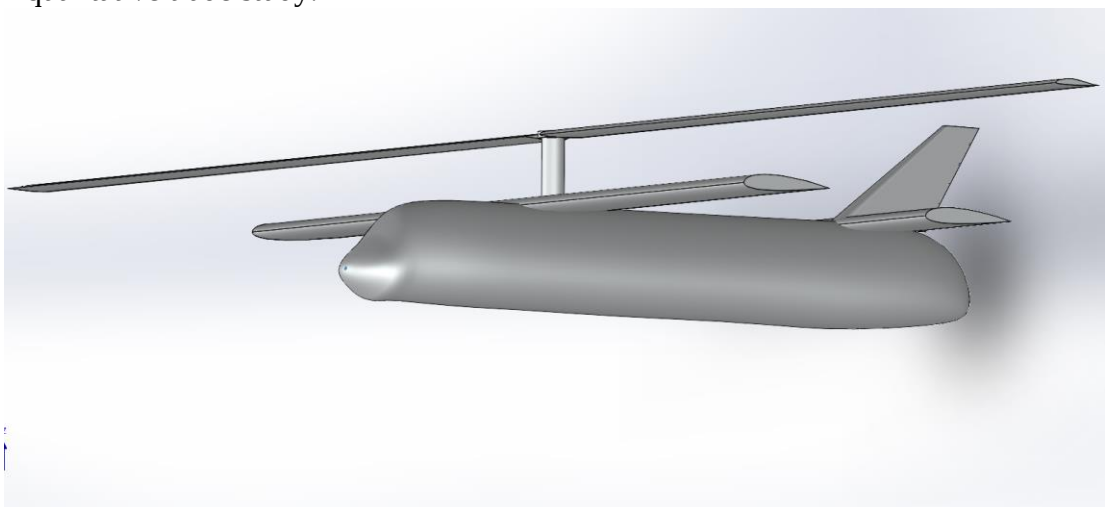

Figure 17 Initial CAD Design

The initial design above shows 12-meter-long rotor blades on top of a traditional aircraft with a high mounted wing. The length was due to an error where only one blade was designed to lift the entire structure. The fixed wings here also did not provide the desired lift and were later lengthened.

4.3) Technique for Order Preference by Similarity to Ideal Solution (TOPSIS)

The technique for order preference by similarity to ideal solution (TOPSIS) is a versatile tool that can be applied to a range of different projects to help with selecting the best possible option. TOPSIS tool works by creating a hypothetical to ideal solution for a specific problem in our case it is selecting the appropriate motor for an Autogiro, then the tool compares the given motors with the hypothetical ideal solution. The TOPSIS tool creates a tailored hypothetical ideal solution based on the customer preference in the form of selecting a weight to each criterion. The best alternative option has the shortest to the positive ideal solution and farthest away from negative ideal solution, the final rank of the options are ranked from closest to one to the closest to zero. Some advantages to using TOPSIS tool that its very simplicity and has indisputable ranking method because it's based on the input values and weights. Some disadvantages of using TOPSIS it heavily depends on the weight's preferences, solution highly depends on the input values for each alternative, criteria have a monotonically decreasing or increasing utility to decision maker.

The below figure displays the different criteria such as peak power, steady power, motor's efficiency, steady torque, steady speed, and speak speed. Also, the four different motors alternatives with each motor's performance inserted in "DATA MATRIX". The "NORMALIZED MATRIX" changes all the values and non-dimensions them or normalized them, which means the inputs are converted to equivalents non-dimensioned values refer to **table 11**.

Table 11 TOPSIS Input Values and Non- dimensioned inputs

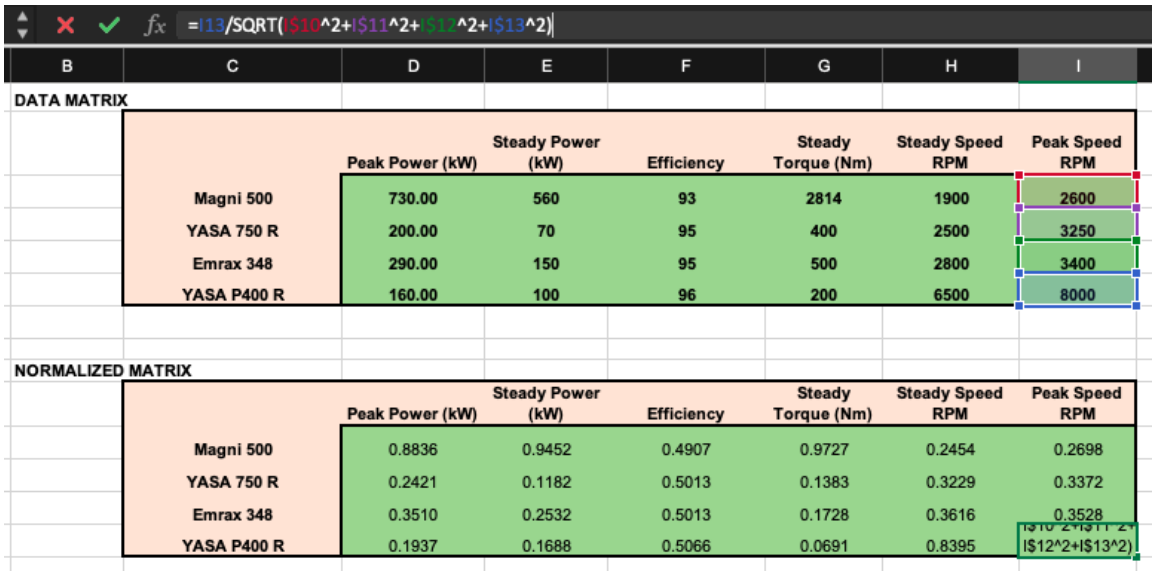

Table 12 below shows the weight preference for each criterion and it being multiplied by the non-dimensioned input values, which yields the "WEIGHTED DATA MATRIX".

Table 12 Criteria Weights

NORMALIZED MATRIX

	Peak Power (kW)	Steady Power (kW)	Efficiency	Steady Torque (Nm)	Steady Speed RPM	Peak Speed RPM
Magni 500	0.8836	0.9452	0.4907	0.9727	0.2454	0.2698
YASA 750 R	0.2421	0.1182	0.5013	0.1383	0.3229	0.3372
Emrax 348	0.3510	0.2532	0.5013	0.1728	0.3616	0.3528
YASA P400 R	0.1937	0.1688	0.5066	0.0691	0.8395	0.8301

CRITERIA WEIGHTS

	Peak Power (kW)	Steady Power (kW)	Efficiency	Steady Torque (Nm)	Steady Speed RPM	Peak Speed RPM
Weights	0.250	0.150	0.100	0.150	0.150	0.200

WEIGHTED DATA MATRIX

	Peak Power (kW)	Steady Power (kW)	Efficiency	Steady Torque (Nm)	Steady Speed RPM	Peak Speed RPM
Magni 500	0.2209	0.1418	0.0491	0.1459	0.0368	0.0540
YASA 750 R	0.0605	0.0177	0.0501	0.0207	0.0484	0.0674
Emrax 348	0.0878	0.0380	0.0501	0.0259	0.0542	0.0706
YASA P400 R	0.0484	0.0253	0.0507	0.0104	0.1259	=I21*I$26

To obtain the positive and negative ideal solutions, first for the positive ideal solution for each criterion selected the highest vales from the four motors. The same goes for the negative ideal solutions select the lowest vales for each of the six criteria refer to **table 13** for more details.

Table 13 Positive and Negative Ideal Solutions Coefficient

WEIGHTED DATA MATRIX

	Peak Power (kW)	Steady Power (kW)	Efficiency	Steady Torque (Nm)	Steady Speed RPM	Peak Speed RPM
Magni 500	0.2209	0.1418	0.0491	0.1459	0.0368	0.0540
YASA 750 R	0.0605	0.0177	0.0501	0.0207	0.0484	0.0674
Emrax 348	0.0878	0.0380	0.0501	0.0259	0.0542	0.0706
YASA P400 R	0.0484	0.0253	0.0507	0.0104	0.1259	0.1660

IDEAL SOLUTION MATRIX

	Peak Power (kW)	Steady Power (kW)	Efficiency	Steady Torque (Nm)	Steady Speed RPM
Positive Ideal	0.2209	0.0177	0.0507	0.1459	0.1259	0.1660
Negative Ideal	0.0484	0.1418	0.0491	0.0104	0.0368	=MIN(I30:I33)

To get the positive and negative ideal solutions, the coefficient of both ideal solutions are multiped by the corresponding weighted data values. After the positive and negative tables are populated the positive ideal solution (S+) and the negative ideal solution (S-) and obtained by taken the square root of the sum of all the criteria values for each of the four motors. The same process is performed to the negative ideal solutions to achieve (S-) refer to **table 14** for more details.

Table 14 Positive and Negative Ideal Solutions

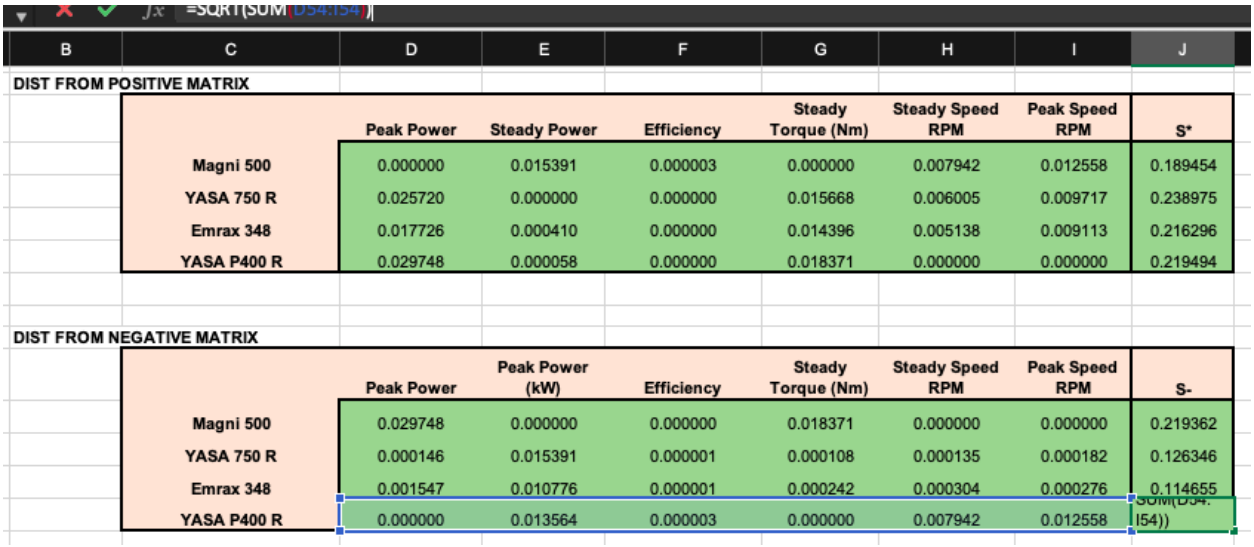

DIST FROM POSITIVE MATRIX

	Peak Power	Steady Power	Efficiency	Steady Torque (Nm)	Steady Speed RPM	Peak Speed RPM	S*
Magni 500	0.000000	0.015391	0.000003	0.000000	0.007942	0.012558	0.189454
YASA 750 R	0.025720	0.000000	0.000000	0.015668	0.006005	0.009717	0.238975
Emrax 348	0.017726	0.000410	0.000000	0.014396	0.005138	0.009113	0.216296
YASA P400 R	0.029748	0.000058	0.000000	0.018371	0.000000	0.000000	0.219494

DIST FROM NEGATIVE MATRIX

	Peak Power	Peak Power (kW)	Efficiency	Steady Torque (Nm)	Steady Speed RPM	Peak Speed RPM	S-
Magni 500	0.029748	0.000000	0.000000	0.018371	0.000000	0.000000	0.219362
YASA 750 R	0.000146	0.015391	0.000001	0.000108	0.000135	0.000182	0.126346
Emrax 348	0.001547	0.010776	0.000001	0.000242	0.000304	0.000276	0.114655
YASA P400 R	0.000000	0.013564	0.000003	0.000000	0.007942	0.012558	SUM(D54:I54))

The last and final step of the TOPSIS tool is to rank the best alternative and the least alternative. The best alternative has the shortest distance from the positive ideal solution, thus the best alternative it's the farthest away from the negative ideal solution and should have a value closest to one. The TOPSIS tool rank them based on each alternative criterion and the least good alternative should have a value closest to zero, refer to **table 15**.

Table 15 Ranking the best Alternative

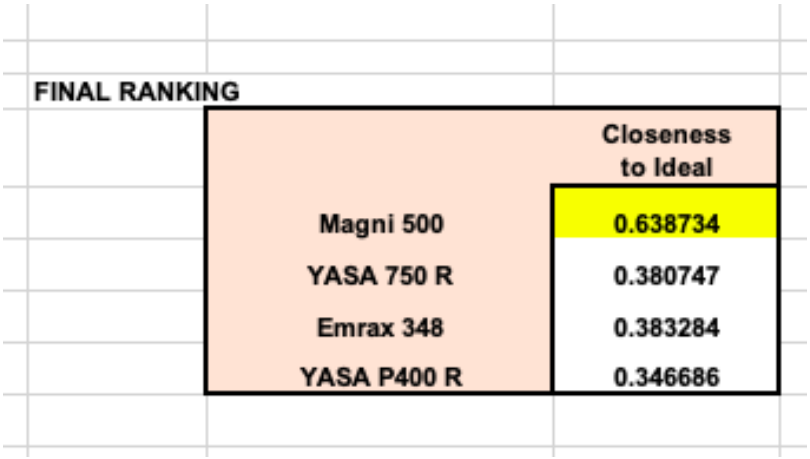

FINAL RANKING

	Closeness to Ideal
Magni 500	0.638734
YASA 750 R	0.380747
Emrax 348	0.383284
YASA P400 R	0.346686

5.0) Chapter 5: Controls and Fuselage Considerations

5.1) Overall Structure

The Flying School Bus Autogiro is envisioned to be flying into crowded urban and suburban areas and as such needs advanced avionics to safely navigate through the sky. Other safety considerations are redundant control methods possible with this type of aircraft. Traditional control surfaces can be in the tail and fixed wings to get pitch, roll, and yaw control. However, other means are available that are unique to the autogiro such as the tilting rotor to control pitch and roll as well as the collective to control climb. Electronic controls would also be implemented such as counter-rotating each wing-tip propeller to provide a net reactive-torque force. IE if the rotor causes a clockwise torque on the fuselage, the propellers can work together to produce a CCW torque to counteract this.

5.2) Rotary Wings

As with many traditional autogiros, the main rotor shaft is not fixed in place. While the tail and wing retain conventional fixed-wing control surfaces, roll, if so desired could also be controlled with the main rotor. This could be done with cyclic control or a tilting head control. The tilting head control was developed and implemented by Cierva himself and is very simple in design [31]. This means of control involves the rotation of the entire rotor-hub assembly to change the orientation of the rotor disk. Traditional types of rotor control are also being looked at as well but due to the simplicity of an autogiro rotor hub in comparison to a helicopter rotor, pursuing a design to emphasize that strength is desirable. However, an in-depth trade studies should be done to have a clear choice. Again, during takeoff and landing, the wing-tip mounted propellers provides the reactive torque needed to account for the torque generated by powering the main rotor.

5.3) Fuselage

The fuselage has a few constraints. One is that the length must be smaller than the diameter of the rotor to keep in-line with traditional design language as well as not be too large to go into crowded areas. It is ideal that the height and width be as small as possible and to aerodynamically have the smallest wetted perimeter (closest to a cylinder). To accommodate for 20 passengers, 10 rows of 2 are required. Based on the standards seen in **Fig. 23**, the minimum width is 44”, minimum height is 60”, and minimum length (not including the cockpit) is 300” for a ‘High-Density / Small Aircraft.’ This fits the purpose of the project, as passengers are not remaining in this aircraft for extended periods of time, and this aircraft does not carry as many passengers as other airlines. The fuselage also has to have a minimum of 12” of space below the cabin floor to hold the battery packs which have the benefit of providing a low center of gravity, further increasing the safety of the aircraft.

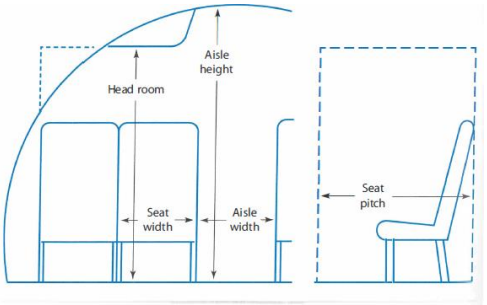

Fig. 9.3 Commercial passenger allowances.

CHAPTER 9 Crew Station, Passengers, and Payload 26

Table 9.1 Typical Passenger Compartment Data

	First Class	Economy	High-Density/ Small Aircraft
Seat pitch, in. {cm}	38–40 {97–102}	34–36 {86–91}	30–32 {76–81}
Seat width, in. {cm}	20–28 {51–71}	17–22 {43–56}	16–18 {41–46}
Head room, in. {cm}	>65 {165}	>65 {165}	—
Aisle width, in. {cm}	20–28 {51–71}	18–20 {46–51}	≥12 {30}
Aisle height, in. {cm}	>76 {193}	>76 {193}	>60 {152}
Passengers per cabin staff (international-domestic)	16–20	31–36	≤50
Passengers per lavatory (40 × 40 in.) {1 × 1 m}	10–20	40–60	40–60
Galley volume per passenger, ft^3 {m^3}	5–8 {0.14–0.23}	1–2 {0.03–0.06}	0–1 {0–0.03}

Figure 18 Standard Sizing of aircrafts based on number of seats [24]

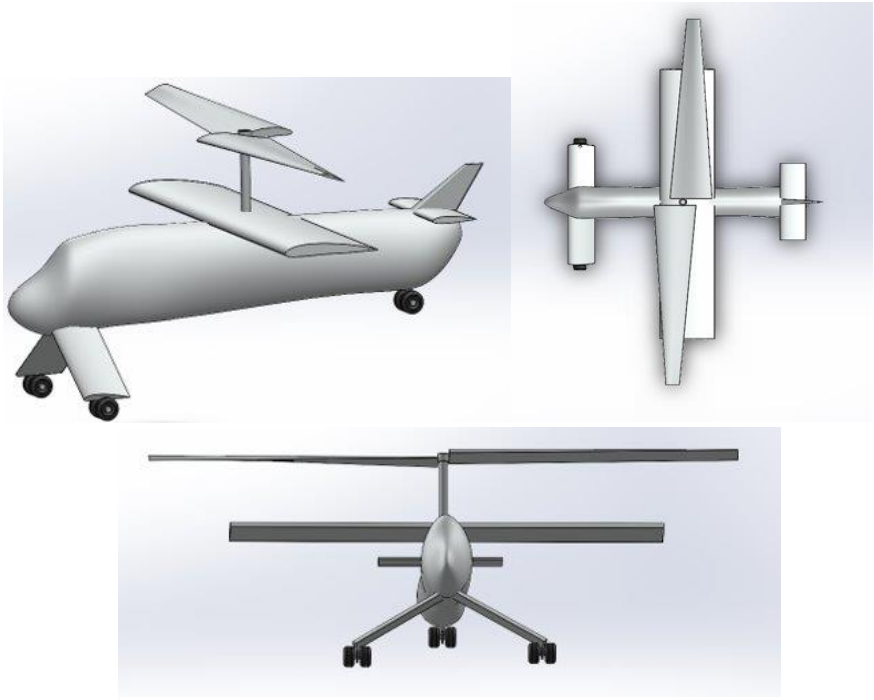

Figure 19 CAD Design Version 2

Version two of the design features a smaller rotor, due to lower weight requirements. A taper of 3:1 and a linear twist was also added to the rotor to increase efficiency [31]. The overall fuselage shape was changed to allow for less drag and to account for the specific inner components, such as the aisle height, seats, cockpit, and battery storage. A tandem-wing design

was explored in this version, as it would allow for more lift and would provide a convenient location for the landing gears. However, there was some concern with the increased tip vortices causing greater loss. As such the next version aimed to remove the need of the secondary front wing via the use of a drastically different rotor.

6.0) Chapter 6: Materials used

6.1) Rotary Wings

Although it would be easier in analysis to create a metal or wooden rotor blade, it is not in common use today for good reason. Wood is suitable for small-scale home-made aircraft. However, it has a host of problems including rot, variation in quality, and susceptibility to damage. Metal blades on the other hand are more durable than wood as well as easier to control for quantity. Corrosion can be an issue as rot is an issue for wooden blades, but both can be accounted for by sealing the structure. The two chief issues for metal is the fatigue life of the blade which limits the life of the blade, and rapid crack propagation from imperfections in the blade's surface. These two issues are inherent to metals and therefore cause attention to be drawn to composite construction.

Composite construction offers many benefits over metal wing construction. Composite structures typically exhibit a higher strength-to-weight ratio, superior damage tolerance and fatigue properties. [27]

6.2) Fuselage

The fuselage is made using with Aluminum alloy. Aluminum is a strong, light, and cheap metal that is commonly used for the body of aircrafts. Typically, a pressurized aircraft has a 2-4mm thick frame however, this autogiro is designed to be unpressurized, as the craft is not flying at high altitude. This means that the thickness may be cut in half, which is why the fuselage, wings, rotor, and tail are all designed with a 1.5 mm thick skin. [25] [26] [28]

7.0) Chapter 7: Weight

7.1) Weight

The first order of business is to establish a maximum allowable weight for the aircraft. This is the number determine the power required, and the size of the rotor. There are a few main parts needed for the aircraft which are broken down Table [16], from here there is given a maximum allowable weight.

Table 16 Weight Breakdown

Parts	Mass (kg)
20 people, each (weight + seat + luggage)	2189.19
3 Magni 500	399.5
6 YASA 750 R	222
140 pack of battery, each (26 kg)	3585.4
Rotor	454.5
Propellers	109.1
Fuselage	2085.9
----------	----------
Total	8586.69

7.2) Weight Distribution

Once all the CAD models were completed, the specific weight density of each material was updated and put into the final assembly. The center of balance was found, and the model was adjusted so that the shaft of the rotor was directly in line with the center of balance. This would ensure that when the rotor was spinning, the aircraft remains in a level and stable flight.

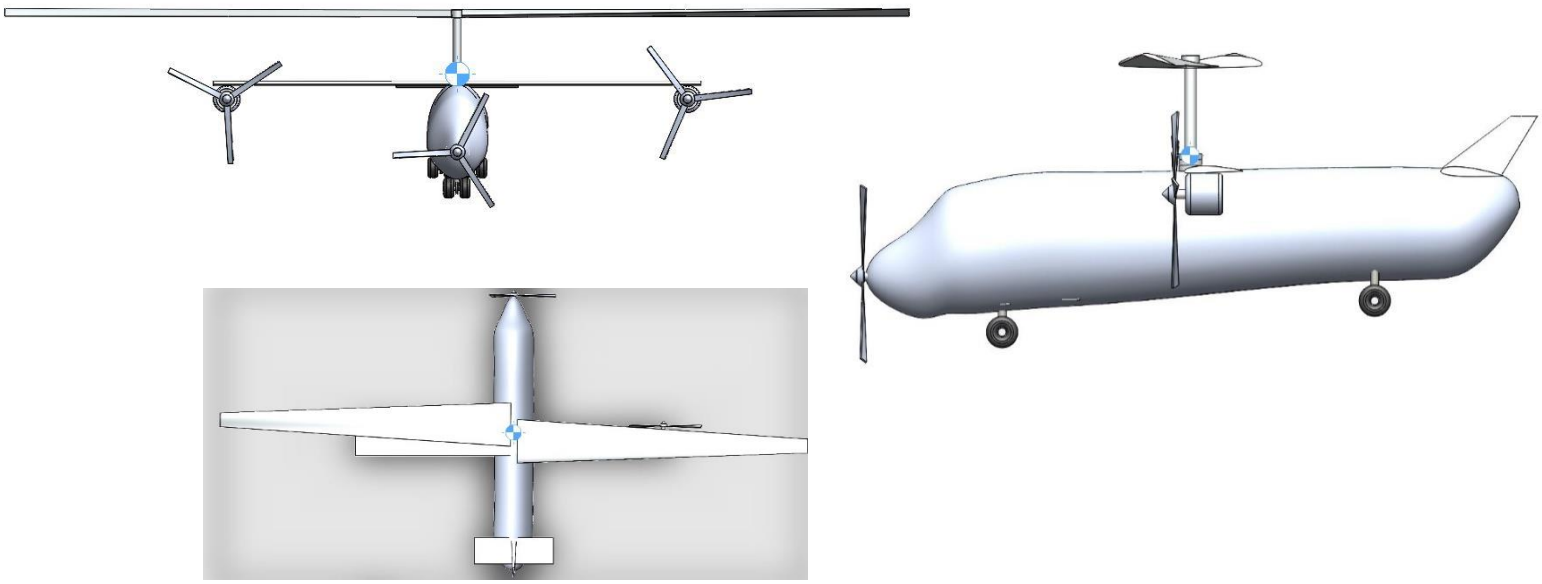

Figure 20 Weight Distribution, the blue and white dot is the center of balance

8.0) Chapter 8: Design Process

8.1) Initial Rotor Calculations

The rotor was designed at first using basic momentum theory calculations. These equations were taken from Leishman [31]. From these calculations the rough dimensions of the rotor as well as power required. However, when the analysis was revisited with blade element theory a clearer picture was gained. It was evident that the size of the aircraft would be too large for a purely electric powered VTOL. Thus, the overall number of passengers was reduced as well as the weight of their allowable luggage. Refining the values using analytical equations from BET:

$$v_i = \sqrt{\frac{T}{2 * \rho * A}}$$

Assuming uniform inflow and at hover, T=weight, rho=1.225, A=area. To find induced velocity at rotor.

$$\lambda = \frac{v_i}{\Omega * R}$$

Finding the inflow ratio. This is also assumed to be uniform over the rotor.

$$C_{l_\alpha} = 2 * \pi$$

We are also able to assume this if flow is assumed to be incompressible.

$$\sigma = \frac{n_b * c}{\pi * R}$$

Finding rotor solidity is a ratio of the area of the blades over the total disk area.

$$C_T = \frac{1}{2}\sigma C_{l_\alpha}[\frac{\theta_0}{3} + \frac{\theta_{tw}}{4} - \frac{\lambda}{2}]$$

Final equation to find the coefficient of thrust. First numerator in brackets is the initial angle at the root with the second numerator in brackets being the rate of change.

$$C_P = \frac{C_T^{3/2}}{\sqrt{2}} + \frac{1}{8}\sigma C_{d_0}$$

From here it is possible to find the coefficient of power. The only variable not yet mentioned is the coefficient of drag assumed to be constant.

Blade Element Momentum Theory: Section 3.3.4 of Leishman [31] gives the equations used in this analysis. Instead of an analytical analysis with assumptions made to simplify the equations, the values here are numerically computed.

$$\lambda(r_n) = \frac{\sigma C_{l_\alpha}}{16}\left(\sqrt{1 + \frac{32}{\sigma C_{l_\alpha}}\theta(r_n) r_n} - 1\right)$$

This equation is for the inflow ratio which is no longer assumed to be constant over the length of the blade. Here theta can be a function of 'r' as well as sigma and C_{l_α}. However, the last two are assumed to be constant. C_{l_α} is assumed to be constant with incompressible flow. It changes over the span, but this can be approximated to 2*pi with minimal loss of accuracy [31]. Sigma is thought to be constant because of the constant chord length throughout the span. Meaning a rectangular planform. 'r' is the nondimensional radius of the rotor blade

$$\Delta C_{T_n} = \frac{\sigma C_{l_\alpha}}{2}\left(\theta(r_n) r_n^2 - \lambda(r_n) r_n\right)\Delta r$$

Here the coefficient of thrust over each blade is found. Here Δr is simply 1/number of stations meaning how many iterations are performed to achieve the desired output. In this analysis, 100 stations were used meaning Δr is 0.01.

$$C_T = \Sigma_{n=1}^{N} \Delta C_{T_n}$$

Finding the coefficient of thrust is simply summing the results of the previous equation. This simply summation implies that the flow over element is uniform but since there are so many elements this is a reasonable assumption to make.

$$C_{P_i} = \Sigma_{n=1}^{N} \lambda_n \Delta C_{T_n}$$

Similarly, the coefficient of induced power is summing the product of lambda and thrust coefficient at each station.

$$\Delta C_{P_o} = \frac{\sigma \Delta r C_{d0}}{2} r^3$$

Finding the coefficient of profile power is found here. C_d0 is an airfoil property. Typically, equal to 0.1 and assumed to be constant over the length of the blade.

$$C_{P_0} = \Sigma_{n=1}^{N} \Delta C_{p_0}$$

Summing the results from the previous equation gives the coefficient of profile power.

$$C_P = C_{P_i} + C_{P_0}$$

The coefficient of power is the sum of profile and induced power coefficients.
Using the same inputs as were used in the BET analytical equations the coefficients of thrust and power were found to be respectively 0.0069 and 0.0008. Thrust and power required were found to be 117.9 KN and 4.89 MW respectively. This total amount of thrust is higher than the weight of the entire aircraft and as such the installed numbers are expected to be lower.

8.2) Second Rotor Calculations

For the second iteration of design, an excel spreadsheet was used to numerically calculate the aerodynamic characteristics of the rotor blade designed for a new, lower vehicle weight. This spreadsheet used 40 stations along the blade, non-linear inflow (BEMT) and used Prandtl's equation to account for tip loss. Also, the newer weight was roughly 67% of the original and this time the number of blades were accounted for when calculating the total thrust of the rotor. With these two major changes, we were able to reduce our overall diameter and power consumption.

It is also important to note the assumptions used in the calculations. Assumptions on the part of the team were that the coefficient of drag was assumed to be constant (0.01) over the entire blade and that there was negligible root loss. Also, Inflow is assumed to be uniform over each blade element. In addition to these user-determined assumptions, many assumptions and limitations are built into the blade element momentum theory. Some of these assumptions and limitations are listed here in no particular order; flow is assumed to be steady and uniform as well as divided into stream-tubes called "strips". These strips are assumed to not affect one another and are essentially isolated from one another. Force and momentum are balanced around this strip providing non-linear equations that can be numerically solved. This is a good theory to use for initial calculations but does require empirical corrections. Said corrections are case specific and might not be applicable. One improved method of analyzing the rotor is using the interactive boundary layer method (IBLM) via XFOIL [35]. Inflow is also analytically found through momentum theory which may break down in certain operating conditions such as low speed forward flight, maneuvers, and descent. Simple unsteady effects can be utilized but are limited [31].

8.3) Current Rotor Design

The current rotor design was made using the same excel sheets used to calculate the first and second iteration. Some major changes were made to the rotor however and the design process behind those changes are detailed here.

First, the rotor was lengthened to lower the disk loading value. This disk loading value was too high at nearly 8 lbs. per square foot. This was halved to 4 lbs. per square foot. Leishman [31] recommends that the autogiro have a disk loading value of 2 lbs. per square foot. However, we decided to keep the value at 4. This is because it would only be applicable during a full power down autorotation landing. During normal operating conditions, the rotor would only be expected to lift roughly half of the total weight which makes the disk loading value equal to 2 which is what is recommended by Leishman.

Second, the twist of the blade was in fact reversed. This is because of the nature of an autogiro rotor blade. For helicopters in powered flight the blades are best served with some twist to help prevent the tips from stalling. The tips are twisted downwards to assist with this. However, in the autogiro the reverse is the case. This is because the incoming air is affected by the rotational speed that the rotor is spinning at. Nearer to the tips the tangential speed is greater due to this rotation. This increased tangential speed means that the air comes in at a shallower angle. To help counteract this the blades are twisted upwards. In this case it is a linear twist from 0 to 9 degrees. Below is a diagram showing what was just explained, tangential is in-plane velocity.

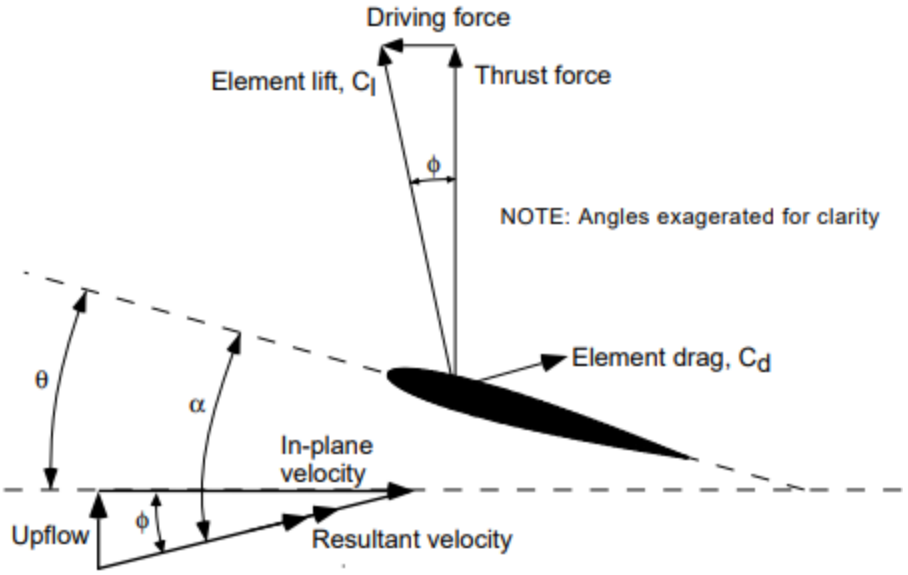

Figure 21 Blade Element in Autorotation Taken from [40]

Finally, there was an addition to the excel sheet for determining the autorotation characteristics of the rotor blade. Varying the degrees of tilt, the rotor was at allowed for controllable amounts of lift. The angles the rotor was tilted at rarely exceeded 4 degrees and would have to have a finely tuned mechanism. Equations used were from Leishman [31], Below is the equation describing the total torque generated by the rotor. In autorotative flight it should be zero because the driving forces are balanced out by the drag.

$$C_Q = C_{Q0} + C_{Qi} = C_{Q0} + k\lambda C_T = 0$$

The inflow ratio is calculated below. The inflow ratio is the ratio of the induced and climb velocities divided by the rotor tip speed.

$$\lambda = \mu \tan(-\alpha) + \frac{C_T}{2\sqrt{\mu^2 + \lambda^2}}$$

The below equation determines the profile torque of the rotor blade. It is based off the viscous drag of the airfoils used on the blade.

$$C_{Q0} = \frac{\sigma C_{d0}}{8}(1 + \mu^2)$$

Advance ratio is the ratio described below. It is important because it represents a limiting factor for all rotary wing aircraft. Most values do not go above 0.5 but autogiros can reach up to 0.7 without a lowering of the L/D ratio of the rotor blade [40].

$$\mu = \frac{V_{forward}}{V_{tip}}$$

Also, descent rates for given forward velocities were calculated in the case of a full power loss scenario. Calculated using the below equation.

$$V_d = \sqrt{\frac{2}{\rho C_D}\left(\frac{W}{A}\right) - V_f^2}$$

Future design methodology includes more rigorous models. Models currently considered are the IBLM utilizing MATLAB XFOIL, a variety of prescribed wake models (Landgrebe, Kocurek Tangler, etc), vortex ring model, rigid/undistorted wake, generalized wake (Beddoes

generalized wake model), and free-vortex wake models as described in chapter 10 of Leishman [31]. A more accessible method of analyzing a blade in autorotation is described by Wheatley [42] and even gives a step by step method of analysis but some properties of the rotor weren't known and as such this author was not able to implement these analyses.

8.4) Propeller Analysis

The propellers were approximated to be ideally twisted rotors with their climb velocities equal to the forward speed at that moment. In this manner the propellers were analyzed using BEMT. The method of analysis was identical to that of the main rotor but less thorough allowing for a simple and quick estimation. The only main difference was in the equation used to describe the twist of the propellers:

$$\theta = \frac{\theta_{tip}}{r}$$

Incorporating the power requirements for the propeller to that of the main rotor the total power requirements were determined and from that the overall range.

8.5) Airfoil

Initially, a characteristic study was conducted for four different NACA airfoils, which were tested for cruise conditions. The main focus of this study is based on the cruise condition altitude because the majority of the flight time is spent at the cruise stage and; thus, that's where the wings are generating mostly half of the craft take-off weight. The airfoils were based on generating the most amount of lift while generating a low drag force relative to the lift force. The initial Lift study was based on a wingspan of 7.14 meters for all four wings, which are NACA 2412, NACA 2415, NACA 4412, and NACA 4415. The cruise speed is 115 knot or 59 m/s at an altitude of roughly 1,500 meters or 5,000 ft.

Meanwhile, the Drag study for the same wingspan of 7.14 m at the same altitude shows that first place goes to NACA 2412, which generated 0.378 KN of drag, second place is NACA 4412, which have a drag force of .413 KN, and the third place is NACA 4415 which generated 0.419 KN of drag force. Moreover, the drag force of the three wings were 41 newtons of difference relatively the first place NACA 2412 and third place NACA 4415. The airfoil that best performed in the cruise condition was the NACA 4412, which is 12 meters in wingspan has produced 57.5 kN of lift and 978 N of drag during the cruise, the parts highlighted in yellow referring to the cruising range and that's how the average lift and drag were obtained refer to **Table 18**.

The following equations were used to calculate the above values:

Lift (L): $L = \frac{1}{2}(C_l * p * v^2 * s)$

Drag (D): $D = \frac{1}{2}(C_d * p * v^2 * s)$

Where each variable is:

C_l is the lift coefficient,

C_d is the drag coefficient,

p is the density of air,

v is the free-stream speed,

s is the surface area of the airfoil

The lift coefficient of each airfoil corresponds to a given angle. In the case of the autogiro the wings are going to be fixed mounted. The angle given in the excel tables is referring to the incidence angle in **appendix D**, **table 17**, **table 24**, **table 25, table 26, table 27,** and **table 28**. The angle of incidence dictates the lift coefficient, based on the lift coefficient, the drag coefficient is given in appendix D titled Airfoil Data on Introduction to Flight

Table 17 NACA 4412 Analysis

Altitude (m)	The Airfoils Lift (N)	The Airfoils Drag (N)
100	22.60643006	0.382570355
200	15.05589877	0.254792133
300	18.32575485	0.310128159
400	47208.70128	798.9164832
500	46752.1142	791.1896249
600	46299.53227	783.530546
700	45850.95548	775.9392466
800	45406.38385	768.4157267
900	44961.81222	760.8922067
1000	44525.25088	753.5042457
1100	44088.68955	746.1162847
1200	43656.13337	738.7961031
1300	43227.58233	731.543701
1400	42803.03645	724.3590783
1500	42378.49056	717.1744557
1600	58073.28696	982.7787024
1700	57502.31058	973.1160252
Average=	57787.79877	977.9473638

8.6) Tail

An empennage consists of a rudder, trim tabs, elevator, horizontal stabilizer, and vertical stabilizer. The empennage is designed to keep a plane stable during the flight as the plane may encounter air flow disturbance. Also, the empennage is designed to maneuver the aircraft safely regardless of the weather's condition, and the weight capacity at take-off. There are many different tail configurations such as: conventional (most common, and light weight), T-tail, cruciform, H-tail, V-tail, Y-tail, twin vertical tail, boom mounted. The Autogiro design is using conventional, all moving tail. The Empennage creates a force that acts upon a lever arm (L_T) which is the distance between the tail aerodynamic center and the CG of plane **Figure 25** [56]. The horizontal part of the empennage creates a moment about lateral axis, and the vertical tail creates a moment about the directional axis (vertical stabilizer). The lever arm of the horizontal

tail (L_{HT}) id the distance between the aerodynamic center of the wing to the horizontal aerodynamic center of the tail. The vertical part of tail or Fin moment lever arm (L_{VT}) which is the distance between the aerodynamic center of the wings to the vertical aerodynamic center of the tail referred to in **Figure 26** [56].

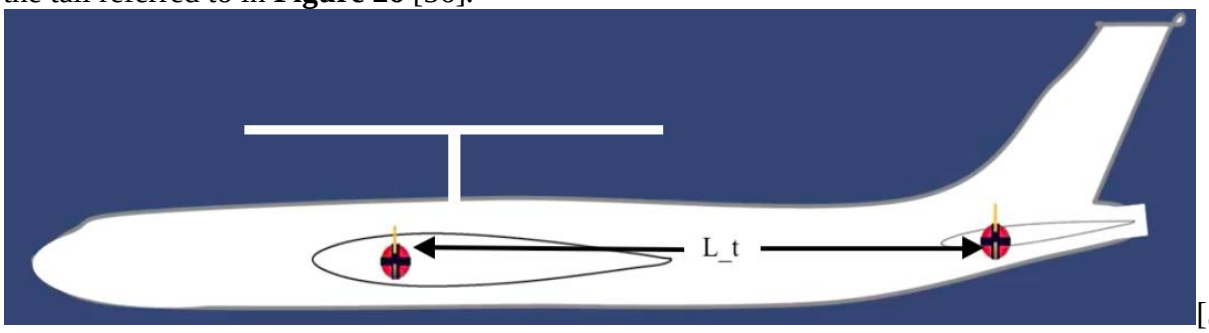

[56]

Figure 25 Moment Tail Arm

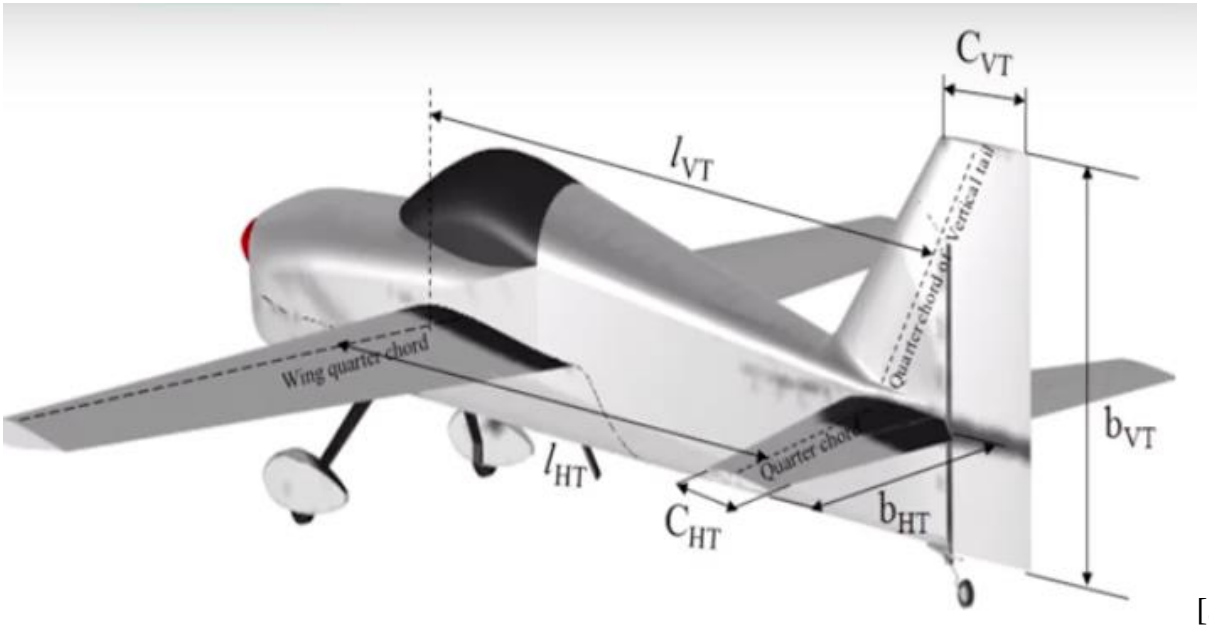

[56]

Figure 26 Moment Tail Arm

The tables below show the empennage calculation which includes the rudder, trim tabs, elevator, horizontal stabilizer, and vertical stabilizer. **Table 18** below, shows the horizontal lever arm (L_{HT}) is 47.5% of the fuselage length (L_f) equal to 10.36 m, thus we obtain the tail lever arm is 4.92 m in length.

Table 18 Lever Moment Arm in % of Fuselage Length (Horizontal)

Tail Arm is 47.5% of Fuselage length	
Fuselage (L_f) (m)	10.36
Lever arm (L_{HT}) (m)	4.921
0.475	

The tables below show the calculation of the vertical lever moment arm length. **Table 19** below, shows the vertical lever arm (L_{VT}) is 44.0% of the fuselage length (L_f) equal to $10.36\ m$, thus we obtain the fin lever arm of $4.56\ m$ in length.

Table 19 Lever Moment Arm in % of fuselage length (Vertical)

Vertical/Fin Arm is 44% of Fuselage length	
Fuselage (L_f) (m)	10.36
Fin Arm (L_{VT}) (m)	4.5584
0.44	

The table below shows the volume of horizontal tail coefficient of 0.8. The area of horizontal tail equation is equal too $S_{HT} = \frac{V_{HT} * S_w * C_w}{L_{HT}}$, where V_{HT} is the horizontal tail volume, and S_w is the wing's area, and C_w is the mean aerodynamic chord. The V_{HT} coefficient is determined to be 0.8 from historical data. After determining the surface area (S_{HT}) of the horizontal tail is calculated using the above equation and (S_{HT}) is roughly $18.5\ m^2$. The aspect ratio was determined from historical data and based on the value the span length (b_{HT}), taper ratio (λ_{HT}), and root chord ($C_{R,HT}$), refer to **Table 20**.

Table 20 Horizontal Tail Volume, Root Chord, and Taper Ratio

Tail Volume Coeff.	
V_{HT}	0.8
Area (S_{HT}) (m^2)	18.51210495
Tail Aspect Ratio	0.502
Span Length (b_{HT}) (m)	3.048454803
Taper Ratio (λ_{HT})	0.35
Root chord ($C_{R,HT}$) (m)	8.996472785
Mean Aerodynamic Chord	
6.541879593	NACA 0009

The table below shows the volume of horizontal tail coefficient of 0.07. The area of vertical tail equation is equal too $S_{VT} = \frac{V_{VT} * S_w * C_w}{L_{VT}}$, where V_{VT} is the vertical tail volume, and S_w is the wing's area, and C_w is the mean aerodynamic chord. The V_{VT} coefficient is determined to be 0.07 from historical data. After determining the surface area (S_{HT}) of the horizontal tail is calculated using the above equation and (S_{HT}) is roughly $6.09\ m^2$. The aspect ratio was

determined from historical data and based on the value the span length (b_{HT}), taper ratio (λ_{HT}), and root chord ($C_{R,HT}$), refer to **Table 21**.

Table 21 Vertical/Fin Tail Volume, Root Chord, and Taper Ratio

Fin Volume Coeff.	
V_{VT}	0.07
Area (S_{VT}) (m^2)	6.090702827
Fin Aspect Ratio	0.301
Span Length (b_{VT}) (m)	1.353994664
Taper Ratio (λ_{VT})	0.33
Tip chord ($C_{R,VT}$) (m)	6.764392698
Mean Aerodynamic Chord	
4.878839425	NACA 0009

8.7) Tail Control Surfaces

The most important point in the empennage section is the control surfaces, which consists on aerodynamic balancing. The hinges on the control surfaces plays a major role in deflecting the control surfaces in various flight conditions. A careful selection of the aerodynamic balancing help reduces the pilot's effort force to control the surface areas about their hinge position. In other words, the electronic control surfaces access it and help the pilot to more the control stick much efficiently when compared to manual controlling. There are several types of tail control surfaces such as but not limited to: set back hinge line, horn balance, internal balance, bevel edge, tab, frise aileron

8.8) Safety

The autogiro on its own is known to be a very safe vehicle. The blades are constantly operating in the autorotative working state where the power to turn comes from relative flow directed upward through the rotor disk. The autogiro also only needs a minimal amount of forward velocity to maintain level flight. If all power was lost, the autogiro would still be able to safely float down, as the main rotor is not powered by anything other than the passing of air through the rotor disk [31]. The autorotative capabilities of a hybrid autogiro are most likely diminished due to the wing which impedes some of the flow into the tip-path-plane during a vertical descent. In forward flight this may not be the case if the angle of the disk, forward flight velocity, and placement relative to the fixed wing allowed for this. Regardless, the rotor may have to be larger than it would be for a pure autogiro. Half of the battery packs are placed under the cabin, and the other half is placed above the passenger's cabins. therefore, providing the entire aircraft with a low center of gravity this makes the aircraft more stable. The battery packs are flammable, however there are many safety measures that can be taken like electric cars. This includes a reinforced structure, improved battery casings, and improved mounting points/locations.

8.9) Issues, Solutions, and Alternatives

This section is to lay out the various problems we were having and the ways we overcame these issues.

WEIGHT: The first major issue was that we were having extremely high-power requirements. Looking at these requirements we realized there was no way for us to power such a heavy aircraft with chemical batteries. So, from here we decided to reduce the number of passengers to 20 and reduce their available luggage to 30 lbs. However, the estimated rotor weight was increased because it had grown to its final size. However, the loss of passenger capacity reduced power requirements which in turn reduced the amount of batteries that were needed lightened the load even more. Fuselage allowable was reduced because much of the weight of the fuselage was accounted for like passengers, seats, batteries, and motors. The team also decided to switch the type of battery to a Panasonic 2170 which has a higher energy density and as such we were able to cut down on the weight as well. It is difficult to find comparable aircrafts to compare the weight of this aircraft to so in the future it would be best to do in-depth structural analysis and design to gain weight through CAD.

TANDEM CONFIGURATION: Even with our lightened load the wing did not make enough lift. Our goal was to have as much lift as possible come from the wing during cruise because of the greater efficiency that would have. To achieve 100% of the needed lift from the

wing it either must get longer which isn't possible if we want to fly in crowded airspace like a city or increase the chord length to the point where it would block the rotor downwash too much. As neither off these options were desirable, we decided to change our wing configuration. Originally it was a single, high-mounted cantilevered beam whereas now it is in a tandem wing configuration. This configuration was inspired by the Rutan Quickie which has a forward anhedral wing that doubles as its fixed, forward landing gear. This can be seen on our model as well. A single rear wheel was added at the rear as a tentative, temporary placement. After this was done it would be possible to have all our lift in cruise be generated by a fixed wing instead of autorotation. As such the autogiro aspect of our design is reduced for efficiency but not lost completely due to the autorotation. Keeping some loading on the main rotor is also desirable as it would promote autorotation if the whole craft were to lose power.

CURRENT CONFIGURATION: Currently, we have decided to allow for a larger single wing and remove the smaller forward wing. The larger single wing was allowable because the rotor blade was lengthened. If the rotor blade is 11.75 meters, then the wing can be made larger if the span of the wing is less than that of the rotor. This is because the team wanted to set the size limit to that of the rotor as it is already so large. Any larger and the viability of this aircraft goes down even more in the applications it is being designed for. Also, the space is already taken up by the rotor diameter and it may as well be used. This configuration is more weight efficient than with two wings. The main wing now produces most of the lift in all maneuvers but descent. This is because the wing causes less drag than the rotor.

POWER: Our final decision regarding the type of power that is used is to keep the aircraft running completely off batteries and not to hybridize the aircraft. With the implementation of the newer Panasonic 2170 batteries the required weight was lower than expected and we were in fact able to increase our range to meet our initial weight guess with batteries. This made the calculation process much easier and increased the effective range of our aircraft. There are two main points here that should be considered. First is that the Panasonic 2170 is not the latest type of battery. As a matter of fact, there is an improved battery that is in the process of being developed for large-scale manufacturing. This would increase our range. Second, is that there is no way for us to verify the results of our fuselage drag at various flight conditions. We are operating on a blind faith when it comes to the fuselage drag as there is no way to analytically/numerically calculate the drag of the fuselage that we know of. The numbers seemed lower than expected and should be further investigated.

9.0) Chapter 9: Results

9.1) Initial Rotor Design

BET Analysis:

Utilizing an excel sheet, the equations from 8.1 were used. The input values were for the number of blades (2), chord length (0.5), lift v alpha slope (2 pi), radius max (11), radius of cut-out (0.1), initial pitch (0.3), pitch equation slope (-0.1396) and RPM (210). This yielded coefficients for thrust and power as described above and they are respectively 0.0039 and 0.00053. This translates to 104.6 KN of thrust and 3.46 MW of power or 4638.7 Hp. The power required was much higher than predicted in momentum theory. As such, a more accurate means of analysis was attempted.

BEMT Analysis:

Using the same values as those used for BET analysis, BEMT analysis was numerically implemented. Code is given in appendix X. Some rough assumptions were considered for the code, but it should still yield a more accurate result than BET analytical equations. Coefficients of thrust and power were found to be 0.0069 and 0.0008 respectively. Thrust found was also slightly higher at 111.4 KN and power at 2.4 MW.

Results Analysis: However, since these results were close to the previous results from BET analysis, the higher power value between the two was selected. This was the main concern of the analysis and a power requirement of ~4600 Hp would be the more conservative estimation. Below are the graphs from BEMT analysis. They should be taken to be rough trends instead of an accurate depiction.

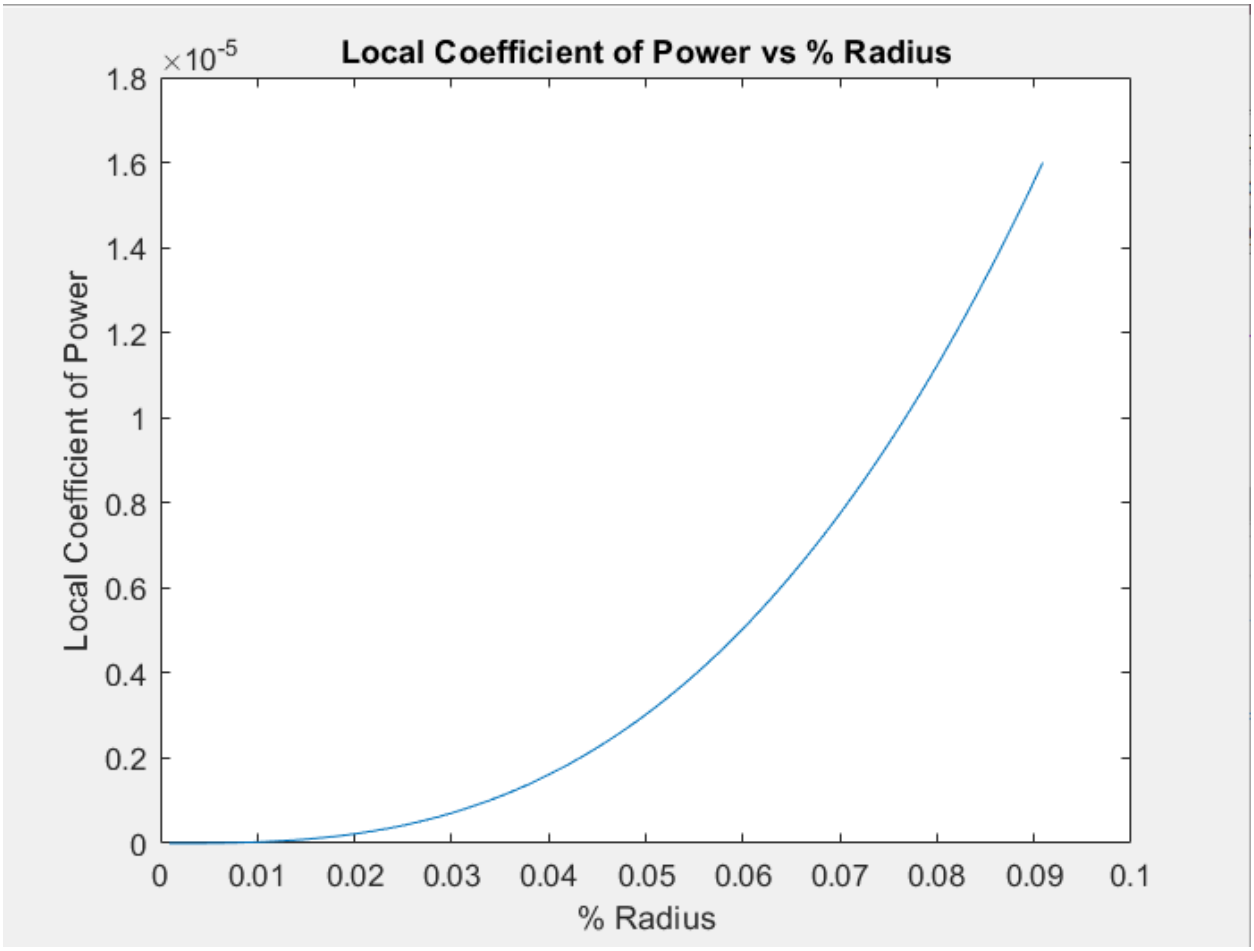

Figure 27 Local Coefficient of Power vs %Radius

The above figure plots the coefficient of power against the radial location of the element. This considers the induced and profile power of each element. As you can see there is no Prandtl tip loss function implemented in this graph.

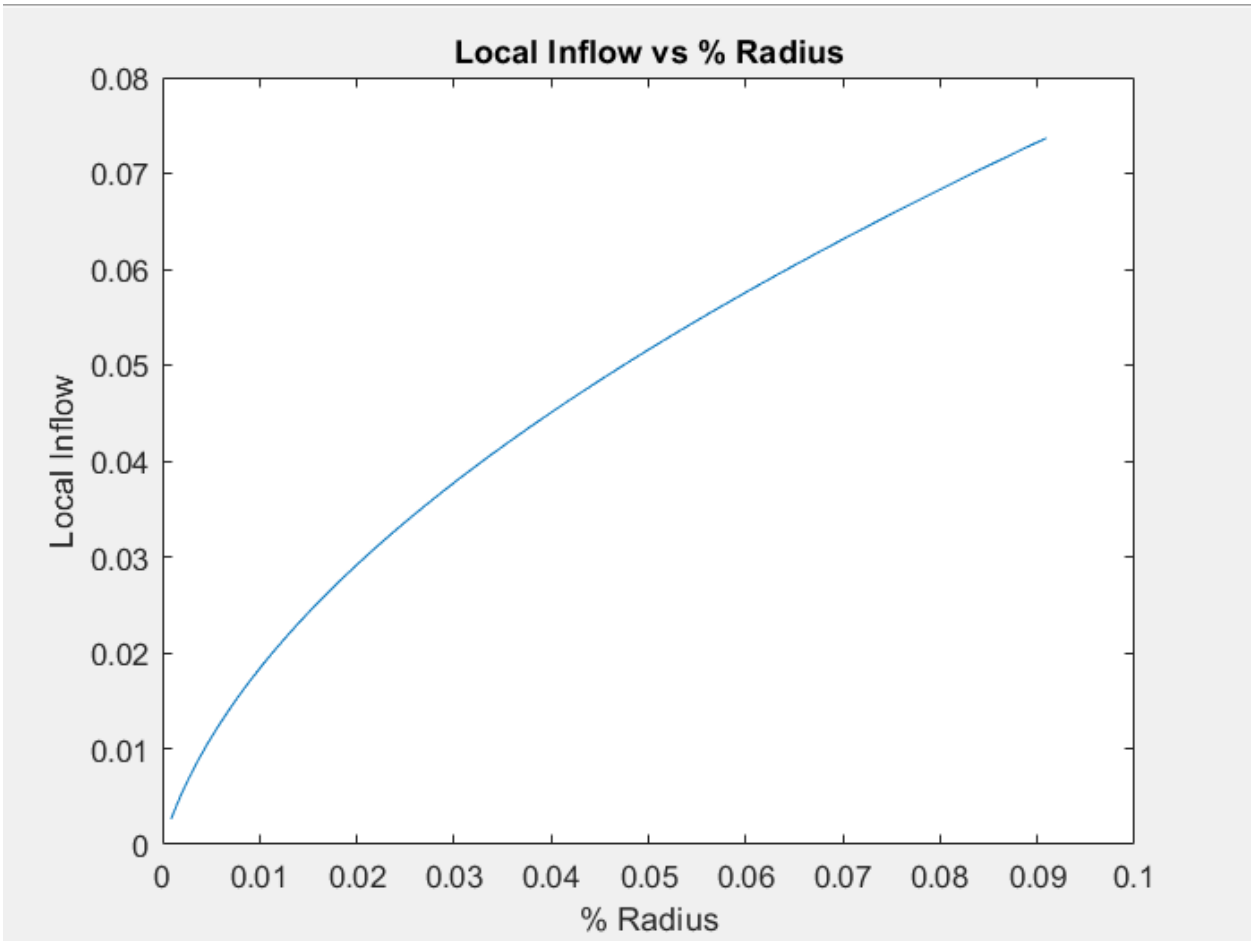

Figure 25 Local Inflow vs %Radius

Here the inflow is plotted against the radial position along the blade. The local inflow is the non-dimensional form of the induced velocity. As you can see the induced velocity grows until the tip of the blade indicating no tip-loss functions are considered.

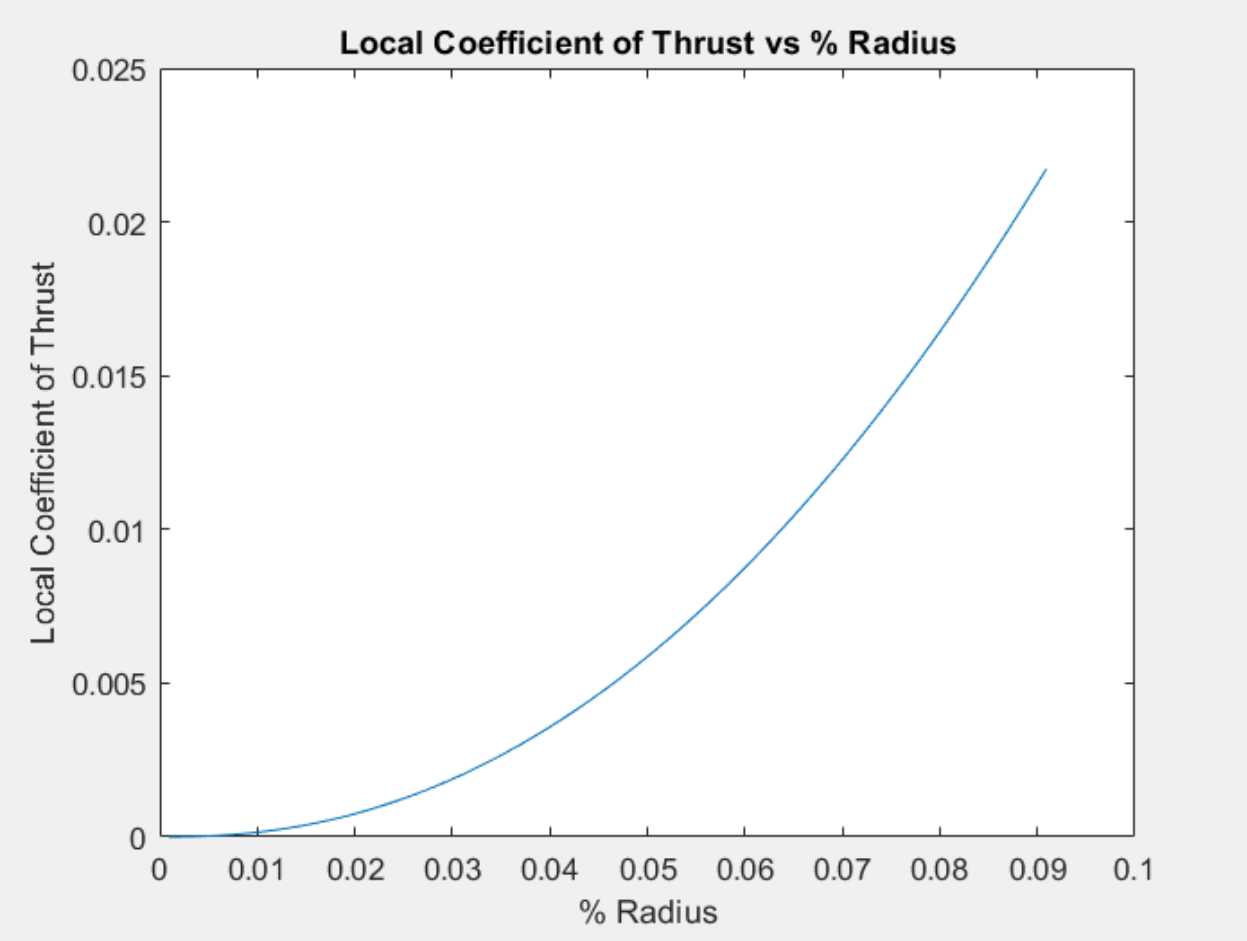

Figure 26 Local Coefficient of Thrust vs %Radius

Related to the inflow is the coefficient of thrust. You can see the trend plotted above against the non-dimensional radial position. The higher the inflow the greater the coefficient of thrust is as well as the coefficient of power. No tip loss accounted for here.

9.2) Second Rotor Design

For the second iteration of design, using the attached excel sheet we were able to determine that the rotor radius would be seven meters and operating at 220 RPM. Power required for hover would be 1407 HP and power for a vertical climb rate of two meters per second would be 1902 HP. It should be noted that these values are only with regards to the main rotor. Down-penalty and anti-torque motors are not accounted for in this estimation. As such we can expect actual power requirements to be greater than what is calculated for hover and climb. Rounding errors due to calculations being done in excel or because there were only 40 elements per blade and not more. Airfoil data was found with a free online database called airfoiltools.com which was the source of various inputs such as the coefficient of drag for the excel sheet [32]. Again, another reason for the drastic drop in power requirements was due to a correction in power calculation. In the first calculation, only one blade was accounted for and as such a single large blade was called for. In other words, when determining the total thrust from its coefficient, the value found was not multiplied by the number of blades. The second iteration of design

accounted for the number of blades in design and as a result drastically lowered the power requirements.

9.3) Current Rotor Design

The current rotor is 11.75 meters in length and operates in VTOL at 140 RPM. The low RPM is to keep a lower decibel rating. It has a 3:1 linear taper with a root chord length of 1.67 meters. The twist is initially 0 degrees and increases to 9 degrees linearly at the tip. Power required in hover is 1272.5 HP. Autorotation characteristics: In a vertical descent, the autogiro is descending at 16.5 m/s. At various levels of required thrust the main rotor can be tilted to generate the appropriate lift. The updated excel sheet is attached to this report.

9.4) Propeller Design

The propellers were analyzed in the same manner as the main rotor. They were approximated as ideally twisted rotors which is a reasonable assumption according to Leishman [31]. Propellers are 3 bladed, 1.5 m radius, 15 cm chord, rectangular planform propellers. They are placed on the wingtips because this allows for the least amount of power needed during VTOL.

9.5) Wing

For the airfoil selection analysis, the lift and drag equations were used to determine and pick the best airfoil out of the selection. NACA 4412 was determined to be the best performing airfoil out of NACA 2412, NACA 2415, NACA 4412, and NACA 4415. The best airfoil was determined based on the highest lift force generated while generating the lowest drag refer to appendix D.2 **Table. 14** and **Table. 15.**

The airfoil that best performed in the cruise condition was the NACA 4412, which is 12 meters in wingspan has produced 57.5 kN of lift and 978 N of drag during the cruise. The cruising altitude is set to be 5,000 ft or 1,500 m with free stream air velocity of $59\frac{m}{s}$ or 115 knots. The parts highlighted in yellow referring to the cruising range where the average of the highlighted values gives the lift and drag forces relatively refer to appendix D.2 **Table. 16** and **Table. 17**.

The second airfoil ranked based on performance from **Table. 14** and **Table. 15** in appendix D.2 was determined to be NACA 4415. The data and calculation of the second airfoil is in **Table. 18** and **Table. 19.** To calculate the lift and drag of both airfoils the same calculation process is the same. The lift equation was used with density changing with altitude and lift coefficient is remains constant throughout the entire flight, the surface area was determined using SoildWorks, and the free stream speed is $59\frac{m}{s}$ or 115 kts. For the drag portion of the calculation the it's the same equation used for lift with the drag coefficient replaced with the lift coefficient.

9.6) Power Calculations

Power calculation results were made by considering all sources of drag including down wash penalties. Finding the propeller power was then calculated for with the results tabulated below. Take-off and landing were approximated to be the same due to the potential for landing to take longer than expected due to external factors. Values are given per propeller. Transient altitude conditions are approximated with the average altitude.

Table 22 Power Requirements at Given Thrust and Altitude

Take-off/Landing

Thrust	3045.8377 N
Altitude	Sea Level
Power Per Propeller	105.506 KW
Thrust Main Rotor	85305 N
Power Main Rotor	1032.856 KW

Cruise

Thrust	1347.481 N
Altitude	1524 m
Power Per Propeller	164 KW

Climb:

Thrust	1629.8083 N
Altitude	762 m
Power Per Propeller	176.076 KW

Descent:

Thrust	1617.12 N
Altitude	762 m
Power Per Propeller	109.0206 KW

Descent power requirements are higher than expected because the wings at this speed generate a negligible amount of lift meaning there is more drag from the main rotor which holding up the entire aircraft. It is also assumed that all propulsive thrust is from the propellers and none from the main rotor although this would not be the case in real life since the main rotor would be tilted forward in a descent. This assumption was done to give a conservative estimation. Another assumption was that it would take the same amount of power in vertical climb and vertical descent. This was for computational simplicity and to give another conservative estimation to account for unknown losses and increased time in-air as compared to the vertical take-off phase.

Taking these power requirements for the propellers and adding in the power requirements for the main rotor in VTOL, the KWH requirements were found. This was done by finding the time it would take to reach our cruise altitude during climb, how long would the vehicle be in VTOL, and how long it would take for the aircraft to descend from cruise. Taking these times and the power requirements from the motors in each phase, the total KWH requirements were found.

They are as follows:

Table 23 KWH Requirements per Flight Phase

KWH Cruise	465.13
KWH VTOL	41.46

KWH Climb	43.99
KWH Descent	18.46
Total KWH	534.615

The total range was found to be 205.082 km or 127.433 statute miles.

10) Chapter 10: CAD Simulations

10.1) Vertical Takeoff

To simulate vertical takeoff, a 1m/s vertical speed was added in the "y" axis, from the bottom to the top of the aircraft. Only the rotating rotor speed of 14.66 m/s was added because that is the only component that will be rotating during vertical takeoff. The flow simulation (figure ---) shows vortices being formed below the wing, which is ideal for takeoff, as this will produce the necessary lift. The streamlines also show that there is no excess turbulence from the rotor.

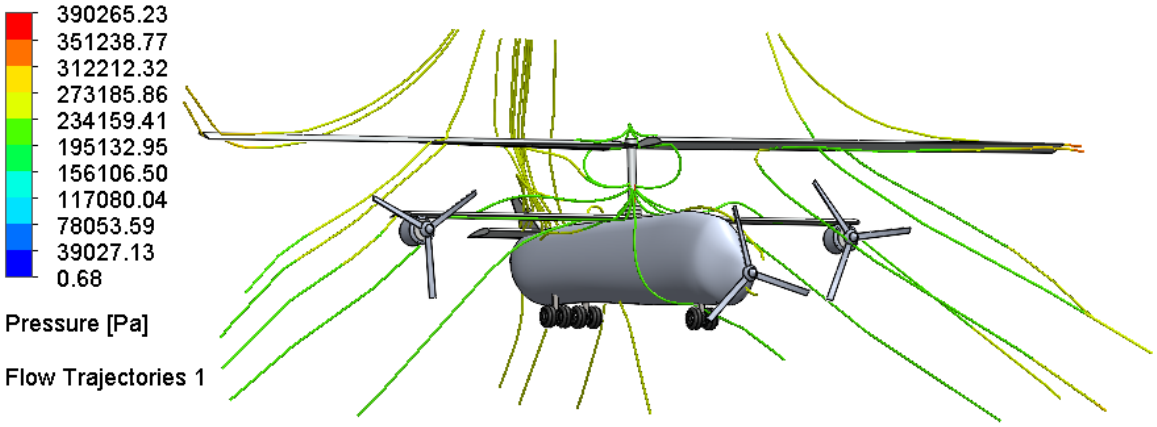

Figure 27 Vertical Takeoff Flow Simulation, the streamlines show the created vortices necessary for lift

10.2) Cruise

An external flow of 59.16 m/s was applied in the "z" direction, from the tip of the aircraft to the tail. Four rotating bodies were inserted. The three propellers rotated at 199 revolutions per second and the main rotor rotated at 14.66 revolutions per second. The flow simulation was then run and the results (shown in figure---) show that the design produces little drag. The simulation does not show turbulent streamlines, all lines are slightly curved, meaning that the design reduces drag while maximizing lift in an efficient way.

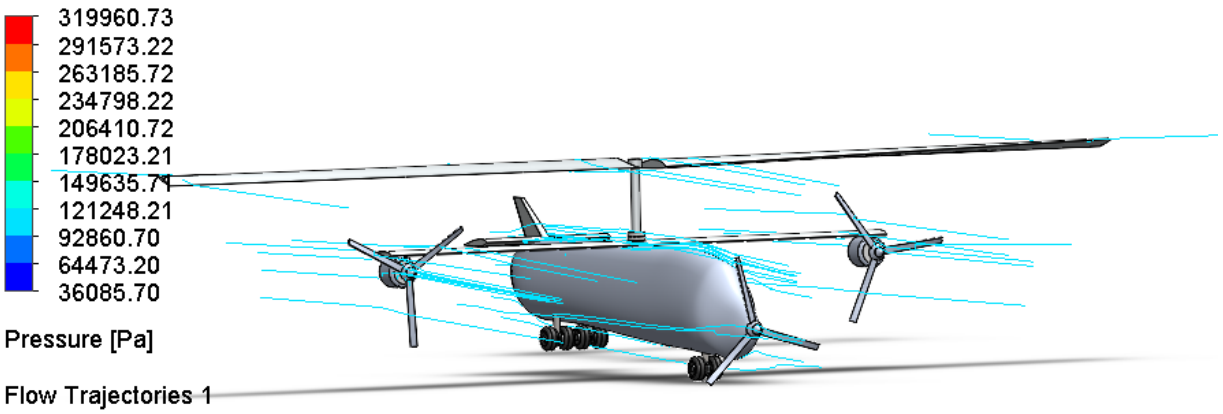

Figure 28 Cruise Flow Simulation, Streamlines are not turbulent

11.0) Chapter 11: Conclusion and Recommendations

11.1) Conclusion

Our conclusion here is that there is a great deal of promise in this approach. The aircraft managed to achieve its goals even when not fully optimized due to the undergraduate level of analysis. The aircraft is capable of inter-city commuting with a passenger capacity of 20. It can get its passengers to its destination at an average speed of about 125 miles per hour safely and reliably, high above the jammed-up highway. Most electric aircraft feature just a handful of seats whereas the relatively high number of seats that we have were deliberately chosen to help defray the costs away from just a handful of customers per flight thus making this mode of transportation more accessible to the middle class. This team believes that if the overall aircraft were to have the same amount of engineering work that modern aircraft do, it would be a viable contender in the urban air mobility market.

11.2) Future Recommendations

Described below are the concerns of the team regarding aspects of the aircraft. It is meant to be a guide to indicate where future efforts in terms of design and analysis ought to be focused and where previous work should be revisited.

Regarding the rotor, the team recommends a further investigation into the overall characteristics of the system. The current radius is 11.75 meters. This is rather large and would there be a way of reducing the rotor radius to help with fitting into city spaces. A more refined design is also needed in terms of airfoils used and taper of the blade. There are currently only two blades meaning that each blade is supporting ½ of the entire load at any given time. It may be more stall resistant to have three or four blades instead of just two. The twist of the blade is also positive which is unusual for a rotor system. This twist should maybe be a double-linear or non-linear twist ought to be used but this must be further investigated. The rotor tip is also not designed and should have some sort of sweep and taper but doesn't and hasn't been designed. Refinement of this would reduce tip losses dramatically which would increase the efficiency of the overall system.

The control of the main rotor can be done in a variety of ways such as a fully articulated hub, a tilt-head rotor, and others. These should be investigated to determine the best compromise between control and weight. The overall weight of the vehicle is heavily determined by the batteries on-board. The main rotor is only powered for short durations and as such, alternative means of powering the main rotor for these short durations should be looked at. As it stands it is powered by a large stack of pancake motors which are dead-weight for most of the flight. Also, would the use of super-capacitors be of any use to powering the main rotor? This author is unsure. Jump maneuvers with the rotor should be determined to see if the takeoff could be powered externally which would remove the need for main rotor motors. Lastly, there are more refined means of analysis [35] for autogiro blades specifically that should be used instead of simple BEMT.

As for the propellers, the team recommends a further investigation into the overall blade characteristics and to do more thorough market research. For example, disk loading parameters typically used in industry should be determined and used in our design. Although difficult to come by, information on currently manufactured propellers should be sought out to make analysis a simple fitting procedure instead of an entire design process. If this process had to go through, the airfoils used as well as the chord, pitch, twist, taper, number of blades, and more

must be determined as well. What kind of propeller system should be used to maximize utility and minimize weight? There are several options such as fixed or variable propellers. The latter of which need a hydraulically powered governor. This means that there will be a higher power consumption that has to be accounted for. There may be a better means of powering this in terms of motor placement and selection that should be investigated as well.

The economics of this aircraft have been determined using very rough and conservative estimations to get an idea of ticket cost to break even in a given timeframe. Further research into the costs of land, facilities, maintenance, manufacturing, and personnel would have to be done to get a better idea of the true costs. Also, the additional cost to type certify a whole new type of aircraft is difficult and expensive which also adds on to the overall cost of manufacturing. Market research into the best placement for highest sales would have to be done as well. What would the taxes and FAA/local/state regulations on this matter be and what would their effect be on the overall viability of the implementation of this aircraft?

The fuselage's shape and size stayed consistent throughout the design iterations. It was based on the number of people it was designed to hold. The final design was three hundred inches long, enough to fit twenty passengers and two pilots in the cockpit. It also had two rows of 10 seats down the length of the fuselage. All the space inside the fuselage was maximized to hold the most amount of battery packs as well as people. One thing we changed was put a few more battery pack above the heads of the passengers, to increase factors such as range and to provide enough power to take off vertically. The size of the seats was made to be the smallest possible width, twelve inches, and this is justified in the sense that though it may not be the most comfortable seat, it is be used only for a very short duration. The seats are also in two single file lines, so people are not squished together side by side, as they are in public transportation. Each seat also has adequate leg room in front of them, as well as additional space under the seat in front of them for an additional carryon bag. Each person is allowed a maximum of one bag with a maximum dimension of 12"x10"x20", which is the size of a typical bookbag. Since this will be used as an alternative to commuting, this aircraft was built under the assumption that people will only be needing one bag for work or school.

The empennage or tail section consists of a rudder, trim tabs, elevator, horizontal stabilizer, and vertical stabilizer. The empennage is designed to keep a plane stable during the flight as the plane may encounter air flow disturbance. Also, the empennage is designed to maneuver the aircraft safely regardless of the weather's condition, and the weight capacity at take-off. There are many different tail configurations such as: conventional (most common, and light weight), T-tail, cruciform, H-tail, V-tail, Y-tail, twin vertical tail, boom mounted. The Autogiro design is using conventional, all moving tail. The Empennage creates a force that acts upon a lever arm (L_T) which is the distance between the tail aerodynamic center and the CG of plane. The horizontal part of the empennage creates a moment about lateral axis, and the vertical tail creates a moment about the directional axis (vertical stabilizer). The lever arm of the horizontal tail (L_{HT}) id the distance between the aerodynamic center of the wing to the horizontal aerodynamic center of the tail. The vertical part of tail or Fin moment lever arm (L_{VT}) which is the distance between the aerodynamic center of the wings to the vertical aerodynamic center of the tail refer to **Figure 25** and **Figure 26** for details. A better-balanced aircraft would require less use of the tail which in turn would reduce the drag of the aircraft and make it more aerodynamically efficient.

The landing gear are fixed. This style very simple and a lot less sophisticated when compared the retractable landing gears. Retractable landing gear are typically much heavier and

requires much frequent maintenance to keep the landing gear operational and still within their safety standers. On the other hand, fixed landing gear typically and not are aerodynamic relative to retractable landing gear because the fixed landing gear generate more drag and turbulence during all flight phases. Since our autogiro design is bulky and big to accommodate the desired amount of people, with big rotor for VTOL, and three motors for thrust, the induced drag is going to be fairly large and adding bit more drag due to the fixed landing gear should affect the autogiro performance by much.

In Summary, there are more details to be worked out. These details are endemic to every facet of the entire aircraft. A lot has been mentioned in the above sections but there are a few things worth mentioning here.

Structural design is not done yet and will have to be done to get a better idea of the costs and weight of the overall design. Rotor control is not designed, propeller/motor mounting and hydraulics for powering the governor, avionics integration, interior design, manufacturing processes, FAA certification costs and other factors that this author is sure are missing have not been accounted for.

12.0) References:

[1] Wikipedia. “Bamboo-Copter.” *Wikipedia*, Wikimedia Foundation, 6 Mar. 2020, en.wikipedia.org/wiki/Bamboo-copter.
[2] Facility, research, and Kiera. “Bamboo-Copter.” *Take Out*, 1 Sept. 2010, researchfacility.wordpress.com/2010/08/20/bamboo-copter/.
[3] Hinder, Charlie, and George Kapff. “Aerial Screw.” *How Have Leonardo Da Vinci's Inventions Affected the World Today?*, 23 Sept. 2013, thedavinciproject.weebly.com/aerial-screw.html.
[4] Apostolo G. “The Illustrated Encyclopedia of Helicopters.” *Amecourt Helicopter - Development History, Photos, Technical Data*, 24 Oct. 2014, aviastar.org/helicopters_eng/amecourt_63.php.
[5] Lambermont, P. “Forlanini - Stingray's List of Rotorcraft.” *Google Sites*, 7 Feb. 2015, sites.google.com/site/stingrayslistofrotorcraft/forlanini.
[6] Clark, Anders. “When Was the First Helicopter Invented?” *Upper Limit Aviation*, 1 Jan. 2016, upperlimitaviation.edu/when-was-the-first-helicopter-invented/.
[7] Chan, Amy. “Juan De La Cierva: Autogiro Genius.” *HistoryNet*, HistoryNet, 9 Jan. 2019, www.historynet.com/juan-de-la-cierva-autogiro-genius.htm.
[8] A. J. Hawkins, "Hyundai will make flying cars for Uber's air taxi service," The Verge, 06 01 2020.
[9] D. Etherington, "Uber Copter offers on-demand JFK helicopter service for top-tier users," techcrunch.com, 06 06 2019.
[10] Electric VTOL News, "skyworks Global eGyro”. Electric VTOL News.
[11] J. A. Mobility. www.jauntairmobility.com
[12] *Kamov Ka-22 “Vintokryl” Helicopter - Development History, Photos, Technical Data* . http://www.aviastar.org/helicopters_eng/ka-22.php .Accessed 26Aug. 2020.
[13] “MagniX.” *MagniX*, https://www.magnix.aero/. Accessed 26 Aug. 2020.
[14] *85-Type | Battery Modules | Products | HSR Motors*. https://hsrmotors.com/products/battery_modules. Accessed 26 Aug. 2020.
[15] *YASA 750 | YASA Limited*. https://www.yasa.com/yasa-750/. Accessed 26 Aug. 2020.
[16] Johnson, Wayne, et al. *Performance of Advanced Heavy-Lift, High-Speed Rotorcraft Configurations*. NASA, 15 Oct. 2007, https://hummingbird.arc.nasa.gov/Publications/files/Johnson_AHSRM2007.pdf.
[17] *Boeing: V-22 Osprey*. https://www.boeing.com/defense/v-22-osprey/. Accessed 26 Aug. 2020.
[18] *Fairey “Rotodyne” Helicopter - Development History, Photos, Technical Data*. http://www.aviastar.org/helicopters_eng/fairey_rotodyne.php. Accessed 26 Aug. 2020.
[19] *GiRos - Products - Gyros-1 (Farmer) - Specifications*. http://www.gyros.su/index.php?action=prod&prod=2&prodact=spec. Accessed 27 Aug. 2020.
[20] Clanton, Nancy. “Study: Atlanta Drivers' Lifetime Cost of Commuting Is Highest in US.” *Ajc*, The Atlanta Journal-Constitution, 11 Dec. 2018, www.ajc.com/news/local/study-atlanta-drivers-lifetime-cost-commuting-highest/7wNFxmrrsD8nB2mdeahLMO/.
[21] Mody, Cyrus C. M. “‘A New Way of Flying’: Différance, Rhetoric and the Autogiro in Interwar Aviation.” *Social Studies of Science (Sage Publications, Ltd.)*, vol. 30, no. 4, Aug. 2000, pp. 513–543. *EBSCOhost*, doi:10.1177/030631200030004002

https://web.a.ebscohost.com/ehost/detail/detail?vid=0&sid=e2f3b297-d7b4-4cf2-a613-d7ab06077709%40sdc-v-sessmgr02&bdata=JkF1dGhUeXBlPWlwLHNoaWImc2l0ZT1laG9zdC1saXZlJnNjb3BlPXNpdGU%3d#AN=5434827&db=a9h
[22] Traum, Matthew & Carter, Rowan. (2005). Pitch Control Benefits of Elevators for Autogyros in Low-Speed Forward Flight. 10.2514/6.2005-26. https://www.researchgate.net/figure/Autogyro-main-rotor-tip-path-plane-incidence-at-minimum-flying-speed-for-A-five-degrees_fig1_268567516
[23] Wang, Song & Chen, Wan & Dun, Wen & Bu, Liang & Dong, Fang. (2016). Design and Experiment of Flight Path Control System of Unmanned Autogyro. MATEC Web of Conferences. 44. 01065. 10.1051/matecconf/20164401065.https://www.researchgate.net/publication/297682884_Design_and_Experiment_of_Flight_Path_Control_System_of_Unmanned_Autogyro
[24] Raymer, Daniel. *Aircraft Design: A Conceptual Approach*. Edited by Joseph Schetz, 6th Edition, American Institute of Aeronautics and Astronautics. Accessed 15 Aug. 2020.
[25] Megson, T. H. G. "Chapter 11 - Structural Components of Aircraft." *Introduction to Aircraft Structural Analysis (Third Edition)*, edited by T. H. G. Megson, Butterworth-Heinemann, 2018, pp. 373–93, doi:10.1016/B978-0-08-102076-0.00011-7.
[26] Sheng, Richard. "Chapter 7 - Systems Engineering Fundamentals." *Systems Engineering for Aerospace*, edited by Richard Sheng, Academic Press, 2019, pp. 113–206, doi:10.1016/B978-0-12-816458-7.00007-7.
[27] Li, Leihong. *Structural Design of Composite Rotor Blades with Consideration of Manufacturability, Durability, and Manufacturing Uncertainties*. 2020-08-20.
[28] "FAA Guide to Low-Flying Aircraft." *FAA*, https://www.faa.gov/about/office_org/field_offices/fsdo/lgb/local_more/media/FAA_Guide_to_Low-Flying_Aircraft.pdf. Accessed 26 Aug. 2020.
[29] *FastStats - Body Measurements*. https://www.cdc.gov/nchs/fastats/body-measurements.htm. Accessed 17 Sept. 2020.
[30] G. Townson, "The Theory of the Autogiro," in Autogiro. The Story of the Windmill Plane, Aviation Heritage, 1985. http://www.aviastar.org/theory/autogiro/index.html
[31] J. G. Leishman, Principles of Helicopter Aerodynamics, New York: Cambridge University Press, 2006.
[32] Degu, Yonas & Alebel, Derbew. (2019). Design of Composite Gyrocopter Main Rotor Blade Involving Rib and Spar Elements. Journal of Engineering, Project, and Production Management. 9. 97-106. 10.2478/jeppm-2019-0011.
[33] Grima Galisteu, Danilo & Adolf, Florian & Dittrich, Jörg & Sachs, Falk. (2015). Simulation Framework for Autogyro OPV Development.
[34] Rezgui, Djamel, and Mark H. Lowenberg. "Nonlinear Blade Stability for a Scaled Autogyro Rotor at High Advance Ratios." *Journal of the American Helicopter Society*, vol. 65, no. 1, Jan. 2020, p. 1. *EBSCOhost*, doi:10.4050/JAHS.65.012005
[35] *Autogyro Rotor Blade for Generating Lift by Autorotation*. 20190523 2019. *EBSCOhost*, search.ebscohost.com/login.aspx?direct=true&AuthType=ip,shib&db=edspap&AN=edspap.20190152594&site=eds-live&scope=site.
[36] Qing, Lin. "Attitude Tracking Control for Autogyro Based on Derivative-Free Adaptive NDI and Dynamic Control Allocation." *2017 36th Chinese Control Conference (CCC), Control*

Conference (CCC), 2017 36th Chinese, July 2017, pp. 523–528. *EBSCOhost*, doi:10.23919/ChiCC.2017.8027396.
[37] Xing Wang, et al. “Refined Performance Results on a Slowed Mach-Scaled Rotor at High Advance Ratios.” *Journal of the American Helicopter Society*, vol. 65, no. 1, Jan. 2020, p. 1. *EBSCOhost*, doi:10.4050/JAHS.65.012003
[32] “NACA 8-H-12 AIRFOIL (n8h12-il) NACA 8-H-12 AIRFOIL - NACA 8-H-12 rotorcraft airfoil,” *airfoiltools.com*. Accessed: 10/15/20. [Online]. Available: http://airfoiltools.com/airfoil/details?airfoil=n8h12-il
[33] “Roof Landings for Autogiros.” *Journal of the Franklin Institute*, vol. 212, no. 2, Aug. 1931, p. 146, doi:10.1016/S0016-0032(31)90846-6.
[34] C. (. Thomas, "Fuel Cell and Battery Electric Vehicles Compared," U.S department of Energy. https://www.energy.gov/sites/prod/files/2014/03/f9/thomas_fcev_vs_battery_evs.pdf
[35] E. Benini, "Significance of blade element thoery in performance prediction of marine propellers," Ocean Engineering, vol. 31, no. 8, pp. 957-974, 2004.
[36] MagniX, "The Future of Flight is Electric," [Online]. Available: https://www.magnix.aero/products. [Accessed 21 10 2020].
[37] YASA, "YASA 750 R," 2020. [Online]. Available: https://www.yasa.com/yasa-750/. [Accessed 21 10 2020].
[38] Cascadia Motion, "PM 150 (150+ KW)," 2020. [Online]. Available: https://www.cascadiamotion.com/productlist/8-inverters/pm-inverters/2-pm150. [Accessed 21 10 2020].
[39] D, John. *Introduction to Flight*. Mcgraw Hill, 2012.
[40] J. G. Leishman, "Development Of The Autogiro: A Technical Persepctive," in *Hofstra University Conference*, Long Island, 2003.
[41] L. S. S. J. a. F. J. R. Jr., "Aerodynamic Characteristics of Four NACA Airfoil Sections Designed for Helicopter Rotor Blades," NACA, Langley Field, 1946.
[42] J. B. Wheatley, "An Aerodynamic Analysis of the Autogiro Rotor With a Comparison Between Calculated and Experimental Results," NACA, Langley Field, 1933.
[43] Gabriel Collins, “The EV Conundrum: High Power Density and Low Energy Density,” Baker Institute Research Presentation, 8 January 2020, Houston, TX
[44] DNK Power, "All Things You Need to Know about 21700 Battery," DNK Power, [Online]. Available: https://www.dnkpower.com/teslas-mass-production-21700-battery/. [Accessed 23 11 2020].
[45] Airbus, Airbus, [Online]. Available: https://www.airbus.com/helicopters/civil-helicopters/Super-medium/h175.html. [Accessed 24 11 2020].
[46] The Convention News Co, "Airbus Helicopters," bjtonline, [Online]. Available: https://www.bjtonline.com/company/airbus-helicopters. [Accessed 24 11 2020].
[47] J. K. O. Balle, "Pratt & Whitney Canada PT6A," FI-POWERWEB.COM, [Online]. Available: http://www.fi-powerweb.com/Engine/PW-CANADA-PT6A.html. [Accessed 24 11 2020].
[48] cityfeet, "Atlanta, GA Commercial Land For Sale," 24 11 2020. [Online]. Available: https://www.cityfeet.com/cont/atlanta-ga/commercial-land-for-sale?sk=eb533e134ded4aa5abd9959bef03e354. [Accessed 24 11 2020].
[49] E. Gazvoda, "Thinking of Building a Hangar?," Business Advisor, 26 12 2017. [Online]. Available: https://www.bizavadvisor.com/thinking-building-

hangar/#:~:text=The%20total%20development%20cost%20for,for%20a%20more%20sophisticated%20facility. [Accessed 24 11 2020].
[50] Southeast Information Office, "Average Energy Prices, Antlanta-Sandy Springs-Roswell," U.S Bureau of Labor Statistics, 11 2019. [Online]. Available: https://www.bls.gov/regions/southeast/news-release/averageenergyprices_atlanta.htm#:~:text=Atlanta%20area%20households%20paid%20an,per%20therm%20spent%20last%20year. [Accessed 24 11 2020].
[51] Ramsden, Todd. An Evaluation of the Total Cost of Ownership of Fuel Cell Powered Material Handling. NREL, https://www.nrel.gov/docs/fy13osti/56408.pdf.
[52] Menzies, Mike. Hydrogen: The Burning Question. https://www.thechemicalengineer.com/features/hydrogen-the-burning-question/.
[53] “Hydrogen Engine.” Pure Energy Centre, https://pureenergycentre.com/hydrogen-engine/.
[54] Szymkowski, Sean. “Why Hydrogen-Powered Combustion Engines Aren’t a Good Idea.” Motor Authority, https://www.motorauthority.com/news/1121008_why-hydrogen-powered-combustion-engines-aren-t-a-good-idea.
[55] NOx Gases in Diesel Car Fumes: Why Are They so Dangerous? https://phys.org/news/2015-09-nox-gases-diesel-car-fumes.html.

[56] “Home.” *WINGS OF AERO*, wingsofaero.in. Accessed 3 Dec. 2020.

VI) Table of Tables in Appendices

13.0) Appendix A - Acknowledgements:

- The team would like to acknowledge professor Adeel Khalid for his insight and assistance throughout the semester. Many technical problems were made easier with his help.
- On the behalf of the Magic Flying Bus we like to acknowledge all the information that help gain more knowledge related to our project in the Reference page.

14.0) Appendix B - Contact Information:

- **Group Members:**
  - **Name:** Hassan Hassan_ **Email:** hassanhassan2@zohomail.com **Phone**: (404) 578- 2222
  - **Name:** Thomas Murdoch_ **Email:** tlmorl1234@gmail.com **Phone:** (407) 485-9550
  - **Name:** Nardeen Saleb_ **Email:** nardeen.saleb@gmail.com **Phone:** (678) 468-0650
- **Advisors and Professors:**
  - Adel Khalid_ **Email:** akhalid2@kennesaw.edu **Phone**: (470) 578-7241

15.0) Appendix C - Reflections:

Thomas Murdoch:

This project turned out to be a bigger challenge than I thought it would've been. A large part of the difficulty was in finding information pertinent our design. It was difficult at every level of analysis. Also, when technical details were finally able to be hashed out there would be large rounds of iteration for each design change and this is just at the undergraduate level of analysis. Also, a large-scale autogiro is not a common sight, and neither are electric aircraft and so the mix of the two made it difficult to find similar concepts. Finding relevant technical data specifically for compound aircraft was not easy either so the team decided to break down the aircraft into its constituent parts and analyze them separately.

Me specifically, I oversaw rotor and propeller design as well as range calculation. I found it very difficult to find information specifically for autogiro rotors and since I was also taking the helicopter theory class at the same time, I was only able to make better design decisions towards the end of the semester. The working state of the autogiro is also not very well understood, and the method of analysis was difficult to come by. In the end a modified momentum theory was used to get a rough calculation of the rotor which is a lower-level analysis than I would prefer but it was the best I was able to do at my level of expertise. It was also very difficult to determine the propellers that should be used and their respective power requirements. Published data of propeller efficiency curves was hard to come by for some reason and in the end the propellers were approximated as ideally twisted rotors with cruise as the perceived climb velocity. I would say this is acceptable for an initial level of analysis as well, but I would've rather gone into further detail. Lastly, the range calculations were done based off my best guest on how to do it. As a matter of fact, the entire process was one of teaching large swathes of information to myself and trying to implement the newly learned information into this hypothetical aircraft.

Overall, I would say that this was a great learning experience especially with forcing myself to learn unfamiliar topics and apply that knowledge immediately. Even with all the difficulties listed above, I was able to find relevant information and apply it to the project.

Hassan Hassan:

This project has turned out way better than initial anticipation, due to the fact that Covid-19 didn't affect our overall plane and that work still got done regardless of the hurtles in our way. My team and I have spent a lot of time reading, rephrasing, and learning tremendous amount of information pertaining to the autogiro design, method of how it would operate, and small details such as the VTOL characteristics and how to design as efficient of an autogiro as possible. The amount of work that was completed for this project was way more work than initial expectations, and that we have learned a lot from doing all the calculation and the necessary designee changes throughout that project.

Nardeen Saleb:

This project was exciting to come up with and execute. It was interesting to see how "in depth" we went in certain chapters. I learned about many new features of Solidworks and I will be able to apply this knowledge in my future career. I believe this is my fourth or fifth aircraft I have designed in Solidworks so it is exciting to see the progress I have made in just two years. This aircraft exceeded my expectations for range, power, and efficiency. I believe that this solution can definitely be implemented, especially in Atlanta, where traffic is a huge issue that

daily occurs. I am thrilled that we were able to power the aircraft through only electricity. I was nervous when we discussed making it hybrid, but by adding another propeller, we were able to successfully accomplish our most important goal. I am very happy with how this project turned out as a whole.

16.0) Appendix D - Supporting Details and Documentations:

D.1) MATLAB Code

The below code was used for the design of the first iteration of the main rotor. It is only capable of analyzing a blade with linear twist and no taper. It does not account for tip losses either. This was meant to be just a quick initial design code and it was.

```
%This code is meant to utilize Blade Element Momentum Theory to calculate
%the coefficients of thrust and power in HOVER for a linearly twisted blade with a constant
chord.
%Equations from Principles of Helicopter Aerodynamics, J. Gordon Leishman 2nd Edition
section 3.3.4
%output is a 2*1 matrix of [coefficient of thrust, coefficient of power]
%Written By
%Thomas Murdoch

function [out]=Numerical_BEMT
r_max=input('enter max radius in meters=\n');
r_cut=input('enter radius of rotor cut-out in meters=\n');
N_b=input('enter number of blades=\n');
a1=input('enter slope of C_L vs alpha (rad^-1) (typically 2*pi) =\n');
c=input('enter chord length (Constant Chord only (in meters))=\n');
rpm=input('enter revolution per minute=\n');
theta_0=input('enter initial pitch for linearly twisted blade in radians\n ');
slope=input('enter slope of equation to describe linear twist, must be negative=\n');
C_d=input('enter the coefficient of drag for the airfoil being used=\n');
rho=input('enter air density value=\n'); %1.225 for sea level
%alpha=input('enter the angle of attack, constant for untwisted blade=\n');
nr=100; %%amount of elements
Area=pi*((r_max-r_cut)^2);
rev=rpm*2*pi/60; %rpm to rad/s

%%Calculating values%%
sigma=(N_b*c)/(pi*r_max); %rotor solidity, rectangular blade

dr=1/nr; %length of span-wise increment along radial
%r1=r_cut:dr:r_max; %radial vector with nr elements and from cut to tip
%r=r1./r_max; %%shift everything to be in the middle for calculation?
r=dr:dr:1;
theta=theta_0-slope*(r./r_max); %%linear twist
%phi=atan(lambda./(r./R);
C_L_a=a1;%*alpha;%*alpha; %assumed to be constant, an assumption without serious loss
%%of accuracy. Assumption also uses the thin airfoil theory results
%and assumes incompressible flow
lambda=(sigma*C_L_a/16)*(sqrt(1+(32/(sigma*C_L_a))*theta.*r)-1);
```

```
%%finding coefficients
dC_T=(sigma*C_L_a/2)*(theta.*(r.^2)-lambda.*r)*dr;
C_T=sum(dC_T);
dC_P=lambda.*dC_T;
C_Pi=sum(dC_P);
dC_PP=(C_d*0.5*sigma*dr).*r.^3;
C_PP=sum(dC_PP);
C_P=C_Pi+C_PP;
out=[C_T, C_P];
Thrust=C_T*rho*Area*(r_max^2)*(rev^2);
Power=C_P*rho*Area*(r_max^3)*(rev^3);
fprintf('your thrust is %g N, power is %g W, and torque is %g Nm',Thrust,Power,Power)



%%Making plots
figure
plot(r./r_max,dC_T./dr)
title('Local Coefficient of Thrust vs % Radius')
xlabel('% Radius')
ylabel('Local Coefficient of Thrust')
figure
plot(r./r_max,dC_P)
title('Local Coefficient of Power vs % Radius')
xlabel('% Radius')
ylabel('Local Coefficient of Power')
figure
plot(r./r_max,lambda)
title('Local Inflow vs % Radius')
xlabel('% Radius')
ylabel('Local Inflow')
```

D.2) Airfoils Data and Calculations

The airfoils candies for the autogiro transport are the NACA 2412, NACA 2415, NACA 4411, and NACA 4415. Each airfoil has a corresponding angle of incidence which was determined for Introduction to Flight book by John D. Anderson Jr. in appendix D "Airfoils Data Tables" [31]. The angle of incidence is the angle between the airfoil relative to the fuselage. Based on the angle corresponding to each airfoil the lift coefficient (C_l) was determined, refer to [**Table. 17**]. After determining the corresponding (C_l) for each airfoil, the drag coefficient (C_d) is obtained refer to [**Table. 25**]. The density of air is at altitude of 1,500 m or 5,000 ft, which is roughly approximated to be 0.8999 $\frac{kg}{m^3}$. The cruising speed was determined to be 115 knots which is about 59 ($\frac{m}{s}$) in SI units. The airfoil's Surface area was determined using SolidWorks CAD software. As we have all the variables needed for the lift and drag equations are obtained, it's time to plug the vibrates in the lift and drag equations and determine the best for airfoil based on their performance.

The results of the four different airfoils selected are shown in **Table 18** and **Table 24**. The table shows the lift force generated by each airfoil. Based on the results in **Table 24**, NACA 4412 generated the most amount of lift of 24.5 kN.

Table 24 Airfoil Selection Lift Profile

Airfoil Selection for Autogyro (Lift)					Wingspan of 7.14 m for all wings
Airfoil Name	**(α) Angle of incidence**	**(C_l) Lift Coefficient**	**(p) Air Density ($\frac{kg}{m^3}$)**	**(V) Velocity ($\frac{m}{s}$)**	**(S) Surface Area (m^2)**
NACA 2412	10°	1.1	0.89994	51.55	15.88085
NACA 2415	11°	1.2	0.89994	51.55	16.11218
NACA 4412	13°	1.3	0.89994	51.55	15.77679
NACA 4415	11°	1.25	0.89994	51.55	16.00812
Total Lift During Cruise	**Results (Newton)**				
NACA 2412	20888.50353				

NACA 2415	23119.39421				
NACA 4412	24524.65441	<-- 1st Place			
NACA 4415	23927.16494	<-- 2nd Place			

Table 25 Airfoil Selection Drag profile

Airfoil Selection for Autogyro (Drag)					Wingspan of 7.14 m for all wings
Airfoil Name	**(C_l) Lift Coefficient**	**(C_d) Drag Coefficient**	**(p) Air Density ($\frac{kg}{m^3}$)**	**(V) Velocity ($\frac{m}{s}$)**	**(S) Surface Area (m^2)**
NACA 2412	1.1	0.02	0.89994	51.44	15.88085
NACA 2415	1.2	0.026	0.89994	51.44	16.11218
NACA 4412	1.3	0.022	0.89994	51.44	15.77679
NACA 4415	1.25	0.022	0.89994	51.44	16.00812
Total Lift During Cruise	**Results (Newton)**				
NACA 2412	378.1718682	<-- 1st Place			
NACA 2415	498.7847109				
NACA 4412	413.2632676	<-- 2nd Place			
NACA 4415	419.3228141				

Table 26 NACA 4412 Airfoil's Data

NACA_4412 Lift profile

Wingspan of 12 meters chord 8%

Altitude (m)	Angle of incidence (α)	Lift Coeff. (Cl) Constant	Drag Coeff. (Cd) Constant	Air Density (p) (kg/m^3)	Velocity (V) (m/s)	Surface Area (S) (m^2)
100	13°	1.3	0.022	1.2133	-1.1	23.69
200	13°	1.3	0.022	1.2071	-0.9	23.69
300	13°	1.3	0.022	1.1901	1	23.69
400	13°	1.3	0.022	1.1787	51	23.69
500	13°	1.3	0.022	1.1673	51	23.69
600	13°	1.3	0.022	1.156	51	23.69
700	13°	1.3	0.022	1.1448	51	23.69
800	13°	1.3	0.022	1.1337	51	23.69
900	13°	1.3	0.022	1.1226	51	23.69
1000	13°	1.3	0.022	1.1117	51	23.69
1100	13°	1.3	0.022	1.1008	51	23.69
1200	13°	1.3	0.022	1.09	51	23.69
1300	13°	1.3	0.022	1.0793	51	23.69
1400	13°	1.3	0.022	1.0687	51	23.69
1500	13°	1.3	0.022	1.0581	51	23.69
1600	13°	1.3	0.022	1.0476	60	23.69
1700	13°	1.3	0.022	1.0373	60	23.69

Average Lift during Cruise => 57787.79877

Average Drag during Cruise => 977.9473638

Table. 26 shows the input values for NACA 4412, consists of Altitude (during cruising condition), the corresponding air density at that altitude, the angle of incidence, lift coefficient based on angle of incidence, drag coefficient, free stream air velocity, and the wing's surface area. **Table 27** shows the total lift and drag of NACA 4412 as a function of altitude. As the autogyro gains altitude (during take-off) the air density becomes smaller as the air gets thinner with altitude. Also, the speed of the take-off is change and adjusted based on the flight

conditions. The portion heighted in yellow refers to the cruise range, which is where the majority of flight is conducted during that range in all provide tables.

Table 27 NACA 4412 Calculation Results

Altitude (m)	The Airfoils Lift (N)	The Airfoils Drag (N)
100	22.60643006	0.382570355
200	15.05589877	0.254792133
300	18.32575485	0.310128159
400	47208.70128	798.9164832
500	46752.1142	791.1896249
600	46299.53227	783.530546
700	47666.66037	806.6665601
800	47204.48363	798.8451076
900	46742.30689	791.0236551
1000	46288.45766	783.3431297
1100	45834.60844	775.6626043
1200	45384.92296	768.0525424
1300	44939.40124	760.512944
1400	44498.04327	753.0438092
1500	44056.68531	745.5746744
1600	43619.49109	738.1760031
1700	43190.62439	730.9182589
Average=	57787.79877	977.9473638

Table 28 NACA 4415 Airfoil's Data

NACA_4415 Lift profile						Wingspan of 7.14 meters
Altitude (m)	**(α) Angle of incidence**	**(C_l) Lift Coefficient**	**(C_d) Drag Coefficient**	**(p) Air Density ($\frac{kg}{m^3}$)**	**(V) Velocity ($\frac{m}{s}$)**	**(S) Surface Area (m^2)**
100	11°	1.25	0.022	1.2133	-1.1	16.00812
200	11°	1.25	0.022	1.2071	-0.9	16.00812
300	11°	1.25	0.022	1.1901	1	16.00812
400	11°	1.25	0.022	1.1787	2	16.00812
500	11°	1.25	0.022	1.1673	5	16.00812
600	11°	1.25	0.022	1.156	7	16.00812
700	11°	1.25	0.022	1.1448	9	16.00812
800	11°	1.25	0.022	1.1337	11	16.00812
900	11°	1.25	0.022	1.1226	13	16.00812
1000	11°	1.25	0.022	1.1117	15	16.00812
1100	11°	1.25	0.022	1.1008	17	16.00812
1200	11°	1.25	0.022	1.09	19	16.00812
1300	11°	1.25	0.022	1.0793	21	16.00812
1400	11°	1.25	0.022	1.0687	33	16.00812
1500	11°	1.25	0.022	1.0581	45	16.00812
1600	11°	1.25	0.022	1.0476	59	16.00812
1700	11°	1.25	0.022	1.0373	59	16.00812
Average Lift during Cruise =>	23911.29615					
Average Drag during Cruise =>	420.8388122					

Table 28 and **Table 29** shows the total lift and drag of NACA 4415 as a function of altitude. As the autogyro gains altitude (during take-off) the air density becomes smaller as the air gets thinner with altitude. Also, the speed of the take-off is adjusted based on the flight conditions. The portion heighted in yellow refers to the cruise range, which is where the majority of flight is conducted during that range.

Table 29 NACA 4415 Calculation Results

Altitude (m)	The Airfoils Lift (N)	The Airfoils Drag (N)
100	42256.40725	743.7127676
200	42040.47572	739.9123727
300	41448.4054	729.491935
400	41051.37	722.504112
500	40654.33461	715.5162891
600	40260.78198	708.5897629
700	39870.71212	701.7245334
800	39484.12503	694.9206005
900	39097.53794	688.1166677
1000	38717.91638	681.4353282
1100	38338.29482	674.7539888
1200	37962.15602	668.133946
1300	37589.49999	661.5751999
1400	37220.32673	655.0777505
1500	36851.15347	648.5803011
1600	36485.46298	642.1441485
1700	36126.73802	635.8305891

D.3) Technique for Order Preference by Similarity to Ideal Solution (TOPSIS)

The technique for order preference by similarity to ideal solution (TOPSIS) is a tool that can be applied to a range of different projects to help with selecting the best possible option. TOPSIS tool works by creating a hypothetical to ideal solution for a specific problem in our case it is selecting the appropriate motor for an Autogyro, then the tool compares the given motors with the hypothetical ideal solution. The TOPSIS tool creates a tailored hypothetical ideal solution based on the customer preference in the form of selecting a weight to each criterion. The best alternative option has the shortest to the positive ideal solution and farthest away from negative ideal solution, which has the final rank of closest to one. Some advantages to using TOPSIS tool that its very simplicity and has indisputable ranking method because it's based on the input values and weights. Some disadvantages of using TOPSIS it heavily depends on the weight's preferences, solution highly depends on the input values for each alternative, criteria have a monotonically decreasing or increasing utility to decision maker.

The below figure displays the different criteria such as peak power, steady power, motor's efficiency, steady torque, steady speed, and speak speed. Also, the four different motors alternatives which are Magni 500, YASA 750 R, Emrax 348, and YASA P400 R with each motor's performance inserted in "DATA MATRIX". The "NORMALIZED MATRIX" changes all the values and non-dimensions them or normalized them, which means the inputs are converted to equivalents non-dimensioned values. Then select the desired weights for each of the six criteria's which the total weights would be equal to one. After determining the desired weights multiply each criteria's value by the "NORMALIZED MATRIX" which yields the "WEIGHTED DATA MATRIX". From the "WEIGHTED DATA MATRIX" rank the lowest as negative ideal solution coefficient and rank the highest to be as positive ideal solution coefficient. To determine the positive (S+) and negative (S-) ideal solutions, multiply the positive and negative ideal solution coefficient by the "WEIGHTED DATA MATRIX". Then to obtain (S+) and (S-) take the square root of the sum of each motor's criteria. Then or the final step of using the TOPSIS tool is to rank the alternative with the highest values closest to one is the shortest alternative from the highest positive ideal solution. Moreover, the best alternative solution should be the farthest distance away from the negative ideal solution refer to **Table. 30**, **Table. 31**, **Table. 32**, **Table. 33**, **Table. 34, and Table 35**.

Table 30 TOPSIS Input Values

B	C	D	E	F	G	H	I
	Qualitative Scale:						
	Excellent	9					
	Above Average	7					
	Average	5					
	Below Average	3					
	Poor	1					
DATA MATRIX							
		Peak Power (kW)	Steady Power (kW)	Efficiency	Steady Torque (Nm)	Steady Speed RPM	Peak Speed RPM
	Magni 500	730.00	560	93	2814	1900	2600
	YASA 750 R	200.00	70	95	400	2500	3250
	Emrax 348	290.00	150	95	500	2800	3400
	YASA P400 R	160.00	100	96	200	6500	8000

Table 31 Non-Dimension the Input Values

NORMALIZED MATRIX

	Peak Power (kW)	Steady Power (kW)	Efficiency	Steady Torque (Nm)	Steady Speed RPM	Peak Speed RPM
Magni 500	0.8836	0.9452	0.4907	0.9727	0.2454	0.2698
YASA 750 R	0.2421	0.1182	0.5013	0.1383	0.3229	0.3372
Emrax 348	0.3510	0.2532	0.5013	0.1728	0.3616	0.3528
YASA P400 R	0.1937	0.1688	0.5066	0.0691	0.8395	0.8301

Table 32 Criteria Weights Times the Non-Dimension Input Values

CRITERIA WEIGHTS

	Peak Power (kW)	Steady Power (kW)	Efficiency	Steady Torque (Nm)	Steady Speed RPM	Peak Speed RPM
Weights	0.250	0.150	0.100	0.150	0.150	0.200

WEIGHTED DATA MATRIX

	Peak Power (kW)	Steady Power (kW)	Efficiency	Steady Torque (Nm)	Steady Speed RPM	Peak Speed RPM
Magni 500	0.2209	0.1418	0.0491	0.1459	0.0368	0.0540
YASA 750 R	0.0605	0.0177	0.0501	0.0207	0.0484	0.0674
Emrax 348	0.0878	0.0380	0.0501	0.0259	0.0542	0.0706
YASA P400 R	0.0484	0.0253	0.0507	0.0104	0.1259	0.1660

Table 33 Obtain the Positive and Negative Ideal Solution Coefficients

IDEAL SOLUTION MATRIX

	Peak Power (kW)	Steady Power (kW)	Efficiency	Steady Torque (Nm)	Steady Speed RPM
Positive Ideal	0.2209	0.0177	0.0507	0.1459	0.1259	0.1660
Negative Ideal	0.0484	0.1418	0.0491	0.0104	0.0368	0.0540

Table 34 positive and Negative Ideal Solutions

DIST FROM POSITIVE MATRIX

	Peak Power	Steady Power	Efficiency	Steady Torque (Nm)	Steady Speed RPM	Peak Speed RPM	S*
Magni 500	0.000000	0.015391	0.000003	0.000000	0.007942	0.012558	0.189454
YASA 750 R	0.025720	0.000000	0.000000	0.015668	0.006005	0.009717	0.238975
Emrax 348	0.017726	0.000410	0.000000	0.014396	0.005138	0.009113	0.216296
YASA P400 R	0.029748	0.000058	0.000000	0.018371	0.000000	0.000000	0.219494

DIST FROM NEGATIVE MATRIX

	Peak Power	Peak Power (kW)	Efficiency	Steady Torque (Nm)	Steady Speed RPM	Peak Speed RPM	S-
Magni 500	0.029748	0.000000	0.000000	0.018371	0.000000	0.000000	0.219362
YASA 750 R	0.000146	0.015391	0.000001	0.000108	0.000135	0.000182	0.126346
Emrax 348	0.001547	0.010776	0.000001	0.000242	0.000304	0.000276	0.114655
YASA P400 R	0.000000	0.013564	0.000003	0.000000	0.007942	0.012558	0.184570

Final Ranking of the Solution closest to the hypothetical Ideal Solution. The alternative closest to the positive idea solution has a distance shortest to the positive hypothetical solution, more over the best positive alternative solution should be farthest away from the negative hypothetical solution. The best alternative solution with a values closets to one is the best alternative and alternative with the least small values from one is considered to the best negative ideal solution refer to **Table 35** for results.

Table 35 Ranking the Ideal Solutions

FINAL RANKING	
	Closeness to Ideal
Magni 500	0.536578
YASA 750 R	0.345848
Emrax 348	0.346441
YASA P400 R	0.456784